A Wave Packet Model for Electron Transfer and Its Implications for the Semiconductor−Liquid Interface

B. B. Smith* and A. J. Nozik

National Renewable Energy Laboratory, 1617 Cole Blvd., Golden, Colorado 80401

Received: March 9, 1999; In Final Form: July 15, 1999

This paper establishes the computational feasibility and examines the implications of a particular technique for simulations of time dependent electron transfer (ET) at semiconductor−liquid interfaces (SLIs). The methodology uses a one electron formalism employing wave packets, pseudopotentials, and molecular dynamics, which we dub WPMD. We describe a detailed mechanism for SLI ET by using the methodology. The model is versatile enough to address conventional SLI ET, surface state and adsorption mediated ET, photoexcited ET, and ET between quantum dots and other microstructures. We contrast the perspectives of our WPMD model of SLI ET with those in traditional literature and find substantial differences. The use of standard Landau−Zener theory for SLI ET is found particularly problematic.

I. Introduction

With the advent of new experimental techniques, processes at the semiconductor−liquid interface can be probed on the picosecond to femtosecond time scale. Results from these new experiments are in acute need of theoretical interpretation.[1,2] Here we present models which highlight the theoretical considerations associated with these ultrafast time scales. The formalism and models developed here can be applied to the new systems of interest in the semiconductor−liquid interface electron transfer (SLI ET) community including those involving dye sensitized and other photoexcited SLI ET, adsorption and surface state mediated SLI ET, and ET between quantum dots and other microstructures.

In this paper we primarily address the standard model system of SLI ET theory—a system in which the redox species are either not adsorbed or so weakly adsorbed that the ET is little affected by the adsorption per se. In these standard models surface-state ET and ET mediation by additional adsorbed species (e.g., solvent, supporting electrolyte, oxygen, etc.) are also assumed to play no significant role. The systems mentioned in the last paragraph are primarily relegated to an Appendix in the interest of space. They will be addressed in separate papers. It is an open question whether the standard model system is truly an accurate representation of any real world SLI system. Studies such as the present are necessary to address this question.

The traditional theory of SLI processes dates from almost four decades ago and thus lacks modern perspectives. We contrast our wave packet models of SLI ET with traditional outlooks, and find substantial differences. The use of standard Landau−Zener models for SLI ET is found particularly problematic.

We will employ below both simple one-dimensional (1D) and full 3D simulations. The latter uses molecular dynamics coupled with full solutions to the one electron time dependent Schrödinger equation for the ET electron (this is our wave packet molecular dynamics (WPMD)). Of most interest here will be the SLI ET transmission coefficient (κ). Our study represents one of the few addressing fundamental issues of this SLI quantity.

II. Background and Homogeneous ET

We now discuss a simple model for homogeneous ET. This will develop features of our wave packet model for SLI ET and point out key differences between homogeneous ET (between two redox species solvated in a bulk solvent) and heterogeneous ET (between a solvated molecule next to a solid electrode). Homogeneous ET concepts are often erroneously transferred to the SLI.

The total wave function for the electronic and nuclear subsystems of any ET system satisfies the time dependent Schrödinger equation. But solving for the full coupled system of vibrational, rotational, and translational states is computationally intractable even for relatively small systems. The usual practice is to assume the nuclear system can be treated classically, and that only a few electronic degrees of freedom require quantum treatment. In this approximation the quantum and classical systems are still connected because changes in electronic distribution affect the nuclear forces, and in turn nuclear motion affects this distribution. Thus a self-consistent solution is necessary for detailed study. We can examine approximately how the nuclear trajectory influences the probability of transition between quantum states by assuming a fixed classical nuclear trajectory—the characteristic assumption of conventional ET theory. We use this assumption in all 1D models herein; some of the 3D models in section 4 contain self-consistency.

We can model homogeneous ET, at a simple level, as ET between two one-dimensional chains of atoms (see Figure 1). To do so we first consider a 1D chain molecule consisting of, arbitrarily, five atoms. We assume a simple local pseudopotential for each atom given by

$$V_i = V_o \exp(-\sigma (x - x_i)^2) \tag{1}$$

where V_o is the "core" potential, σ is the decay constant for the potential, x is an arbitrary point on the one-dimensional axis, and x_i is the atomic center. We show in Figure 2 the eigenvalues for the stationary states (eigenstates) of this 1D, five-atom molecule using parameters given in the figure caption. Note

10.1021/jp990836s CCC: $18.00
Published on Web 10/21/1999

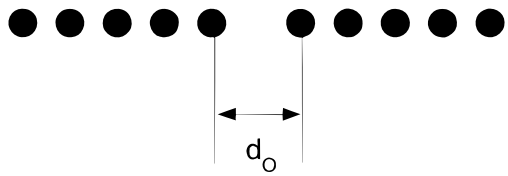

Figure 1. Schematic picture of the two 1D chains of atoms used to model homogeneous ET. The separation between the atomic centers of their adjacent ends is denoted as d_o.

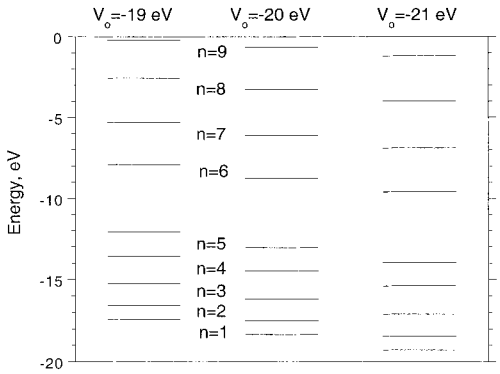

Figure 2. The eigenvalues of the five-atom molecule using $\sigma = 0.69$ Å^{-2}, $d_o = 2.3$ Å, and $V_o = -19$, -20, and -21 eV on *all* redox species atoms.

the shift in the eigenvalues is basically proportional to the change in V_o for this uniform change in V_o on all redox species atoms.

Let us place two of these five-atom molecules next to each other with a separation of d_o between their adjacent ends (see Figure 1). We assume the potential in the electronic Hamiltonian for the system of interest is simply a linear superposition of the atomic pseudopotentials, i.e.

$$V_{\text{system}} = \sum_i V_i \tag{2}$$

where V_i is given by eq 1. This is typically termed the empirical pseudopotential method,[3] where in system specific calculations the atomic pseudopotentials are adjusted to fit experimental and ab initio data. In all of our 1D models we do not sum over solvent atomic sites in eq 2; our present homogeneous model sums only over redox species sites. That is, we assume the penetration of electron density into the solvent is negligible. No solvent is assumed between the two redox species although such a 1D potential could be introduced. Indeed in our 1D models the solvent will only be accounted for in one way, as follows. As the polar solvent changes its configuration, the electric field acting on the redox species obviously changes. For simplicity we assume this electric field operates only to change V_o for the redox species. Since we assume the classical nuclear trajectory is fixed, these V_o will be a fixed function of time. Realistic pseudopotentials and dynamical effects are reserved for the 3D models. The 1D models are essentially pedagogical.

In the traditional homogeneous ET conceptualization, the polar solvent (and redox species) must adopt a configuration via random thermal motion which yields an electric field acting on the redox species such that the energy of the system is the same when the electron is on either species. This typically defines the traditional ET transition state (TS).[4] Let us now assume our system in Figure 1 has a solvent configuration that yields this degeneracy, and in our present simple model we institute this by setting V_o equal on each redox species' atomic site. We now place a wave packet (a spatially bounded wave function) in what would be (in absence of the right-hand molecule) a stationary state of the left-hand molecule in Figure 1. We use eigenstate $n = 6$ for illustration (see Figure 2) and solve the time dependent Schrödinger equation

$$i\hbar\partial|\psi\rangle/\partial t = \mathrm{H}'|\psi\rangle \tag{3}$$

for this two-molecule/one-electron system using numerical techniques (see Supporting Information Appendix S.1). Our electronic Hamiltonian is

$$\mathrm{H}' = (-\hbar^2/(2m))\nabla_x^2 + V_{\text{system}} \tag{4}$$

with V_{system} given by eq 2.

Under the conditions just described (two molecules with identical eigenstates), we have a resonance condition set up and the wave packet initially placed in eigenstate $n = 6$ of the left molecule in Figure 1 simply oscillates back and forth between this same eigenstate in the two molecules with a given frequency (see Figure 3a). This resonance frequency is given, approximately, by the familiar equation, $\omega \sim |V|/\hbar$, where $|V|$ is the electronic coupling matrix element for the two states.[5] Figure 3b shows the oscillatory time dependence of the electron/probability density, n_{REDOX}, on the left redox species (n_{REDOX} is calculated by summing the probability density over the length of the redox species).

So far we have assumed the solvent has a fixed configuration, i.e, that the V_o are constant in time. But the time dependence of this configuration is key to ET. There is an average electric field that acts on the redox species when the solvent is in equilibrium with it. But occasional large fluctuations of the configuration and the associated electric field (and short-range potentials) cause ET because they enable the system to reach the TS. Let us take the $n = 6$ eigenstate to approximate the state associated with ET for a redox species in equilibrium with the solvent. Let us assume the reduced redox species has on average an eigenvalue for this state 2 eV different than the corresponding oxidized species eigenvalue. We set all of the V_o for the reduced left molecule about 2 eV below the right to represent this equilibrium situation. We then assume that during a fluctuation that *all* V_o on the left and right molecule change by the same amount, but oppositely, linearly in time (see inset in Figure 4). Initially we place a wave packet in the $n = 6$ stationary state of the left molecule, as before. Figure 4 shows the resulting time dependence of n_{REDOX} on the left redox species. As we increase the rate of change of V_o there is less time spent in the degenerate region (the TS) and the amount of ET is less, as Figure 4 shows. If we stop the change in V_o where the same degenerate V_o values used in Figure 3 are reached we get the same kind of oscillation seen in that figure. In this homogeneous system, oscillation influences the ET in both the static and dynamic case, as we will see in detail below.

The famous Landau−Zener (LZ) model of curve crossing, a two-state model, also assumes a fixed nuclear trajectory. Landau and Zener independently derived the same analytical expression for p, the probability of staying on the initial diabatic energy curve in a passage through the crossing point (the region of eigenvalue degeneracy, i.e., high electronic coupling).[6−8] Zener's time dependent Schrödinger equation derivation is most pertinent. He assumed that the diabatic eigenvalues changed linearly with time so that[9]

$$(\epsilon_2 - \epsilon_1)/\hbar = \alpha t \tag{5}$$

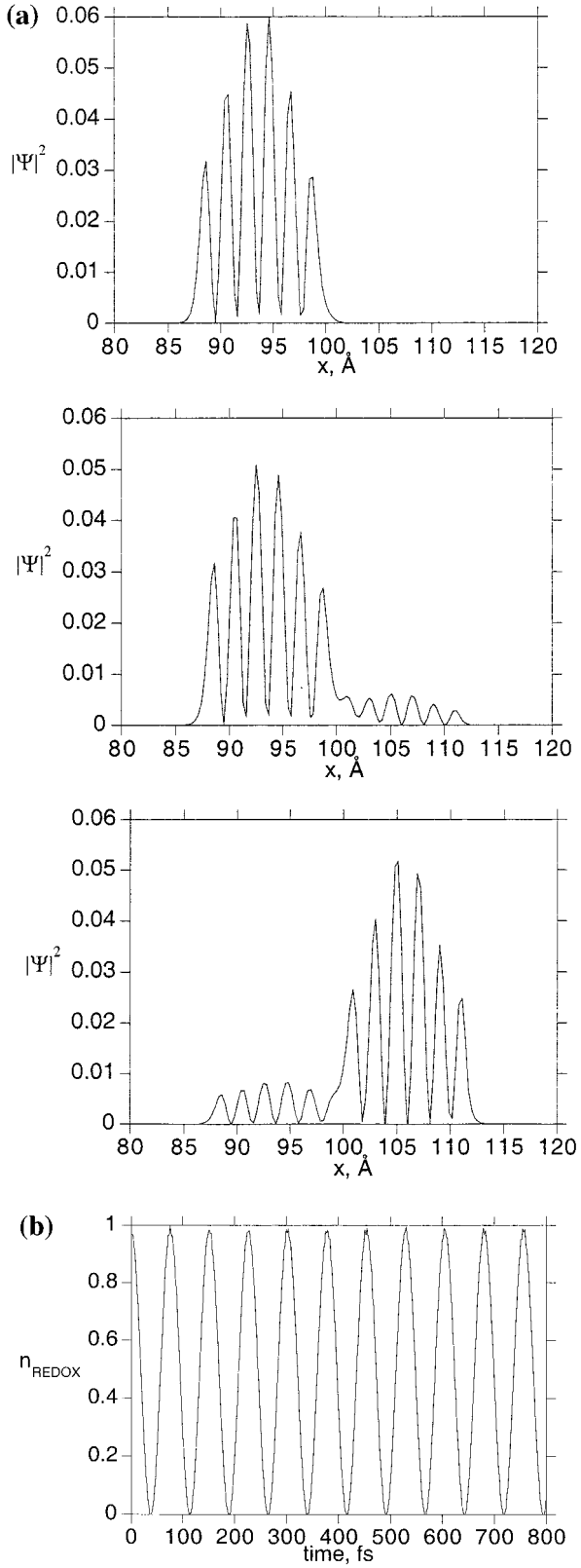

Figure 3. (a) The wave packet initially placed in eigenstate $n = 6$ of the left molecule in Figure 1 simply oscillates back and forth under these resonance conditions (see text). (b) Variation of n_{REDOX} on the left molecule with time for the same conditions as in (a). Here, d_o was about 2 Å and V_o for all atoms on both species was about −20 eV, resulting in the high oscillation frequency (and electronic coupling) shown in the figure.

where α is a constant. This is approximately the equation the diabatic eigenvalues of our system obey when we change V_o linearly as above. If the electronic coupling matrix element is

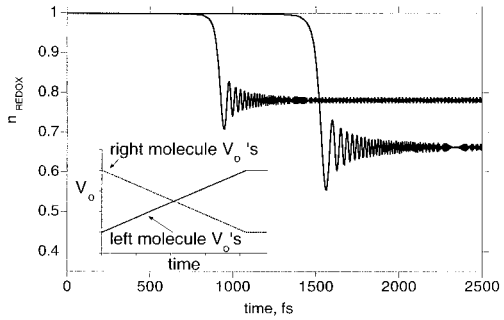

Figure 4. Shown is the time dependence of n_{REDOX} on the left redox species resulting from an imposed time dependence of V_o on the two molecules (shown in the inset). The rate of change of V_o for the lower n_{REDOX} curve is less than that of the upper, while the change in magnitude of the V_o is the same. Here, d_o was about 1. Å more than in Figure 3, hence the time scales are longer.

assumed constant in time and a number of other assumptions are made (listed in appendix A), Zener showed that[6,8,9]

$$p = \exp(-2\pi\gamma) \tag{6}$$

with

$$\gamma = |V|^2/(\hbar|(\mathrm{d}(\epsilon_2 - \epsilon_1)/\mathrm{d}t|) = |V|^2/(\hbar^2\alpha) \tag{7}$$

where eq 5 is used to obtain the last equality in eq 7. Equation 6 was obtained by Zener by calculating the occupation probability for a species in the long time limit after one crossing (after an initial crossing occurs and before a second arises). For our system just discussed, this is equivalent to n_{REDOX} in the long time limit for the left molecule, i.e., $p = n_{REDOX}(t \rightarrow \infty)$ for a *single* eigenvalue crossing. In regimes where the simple LZ model assumptions (see appendix A) are applicable, the LZ p (eq 6) matches our results if we consider only a single crossing. Let us call P the probability of electron transfer to the other redox species, given that the TS is reached. For a *single* crossing this ET transition probability, P, is just equal to $1 - p$ ($P = 1 - n_{REDOX}(t\rightarrow\infty)$).

So far we have considered just one crossing. If the trajectory of the ϵ_js in time makes two or more crossings into regions of high electronic coupling (where the eigenvalues are nearly degenerate), quantum interference (QI) arises. For example, we might have a time dependence of the form

$$(\epsilon_2 - \epsilon_1)/\hbar = \alpha(t - t_o)^2 + B \tag{8}$$

instead of eq 5. The interference arising from electronic coherence makes P an oscillatory function of α when multiple crossings occur. We indeed see oscillations in P as a function of α with our model when we use eq 8 for the time dependence of $\epsilon_2 - \epsilon_1$. We have verified that we obtain Stueckelberg's QI model (which uses eq 8) results for P in regimes in which that model is appropriate.[8,10] QI will be important in comparisons of solid−liquid and homogeneous ET in section 5.

The traditional first order homogeneous ET rate constant is described by transition state theory (TST) using the familiar Arrhenius-type expression

$$k_{ET} = \kappa k_{TST} = \kappa(\omega_r/2\pi)\exp(-\Delta G^{\ddagger}/k_B T) \qquad (\Delta G^{\ddagger} = (E_r + \Delta G^{\circ})/(4E_r) \tag{9}$$

where k_{TST} is the transition state theory ET rate constant;[11,12] ω_r is the appropriate reaction coordinate (angular) frequency inside the metastable minimum (in a modern interpretation);[13]

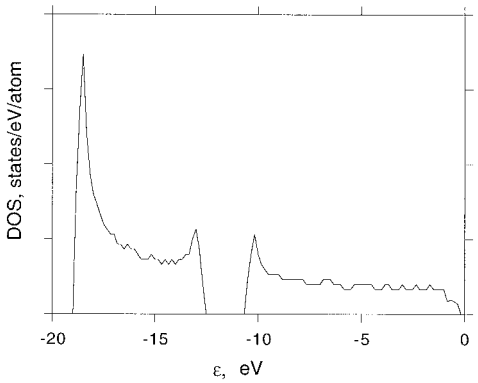

Figure 5. The DOS for the 1D semiconductor model we employed for the parameters given in the text.

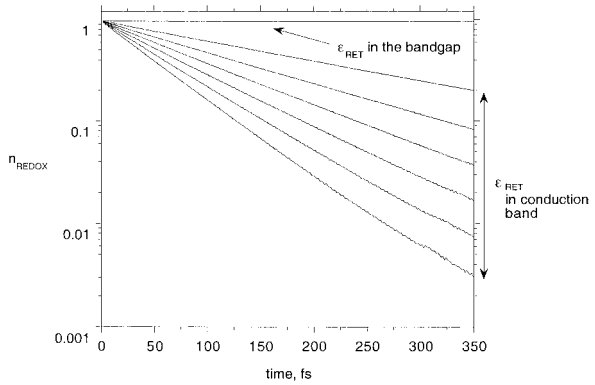

Figure 6. n_{REDOX} as a function of time under fixed V_o conditions for the SLI oxidation case. Here, d_o was about 2.5 Å. The highest curve was for a ϵ_{RET} in the band gap. For the other curves ϵ_{RET} varied from about 0.01 eV above the band edge (second to the highest curve) to about 2. eV above the band edge for the lowest curve (for our system curves have more rapid decay the higher they are in the band due to changing electronic coupling). We have also seen significant variation in coupling over smaller energy ranges (more characteristic of SLI ET, see eq 14).

$\Delta G^{\ddagger}$ is the electron transfer activation energy which is the function shown of the reorganization energy, E_r, and the reaction free energy, $\Delta G°$;[11,12,14] and κ is a correction to TST (TST assumes $\kappa = 1$). Perhaps the most often used expression for the ET κ comes directly from LZ theory, as next discussed.

To relate their model to reaction coordinates Landau and Zener assumed that the diabatic eigenstates ϵ_2 and ϵ_1 in eq 5 were a function of a single nuclear coordinate R and that this dependence was linear near the crossing region (the only region where LZ is strictly valid, see Appendix A). Since the two-state model and a single reaction coordinate also form the foundation of traditional ET theory,[4,12] the LZ model can be used for κ, as detailed in Appendix A. In simple terms, κ is just the probability of ET once the TS is reached, thus in the LZ framework by definition $\kappa = P$ (see above). We will see specific expressions for $\kappa = P$ as a function of p in section 5. We now begin to examine why a two-state model, in general, appears inadequate for solid−liquid ET.

III. SLI ET (1D Models)

The traditional expressions for the first order local SLI ET rate constant (as contrasted to the second order rate constant[15]) are no different than the homogeneous expression (eq 9); in essence, only the parameter E_r is changed.[16] Of most interest to us here is the quantity κ in eq 9. Traditional SLI ET theories, including Gerischer's, offer no expression for it,[16] and the practice has generally been to use homogeneous κ expressions (e.g., eqs 12, 13) for the SLI κ. The latter is highly problematic because the SLI system is very different than homogeneous ET systems, as we begin to illustrate next.

In this section we extend our homogeneous model to describe SLI ET, which will serve to point out key differences between the two systems. We use the same basic pseudopotential model as in section 2. But we now regard the chain on the right in Figure 1 as the semiconductor and the chain on the left as the redox species. We make the chain on the right longer to model the semiconductor (600 atoms were typically employed). For the interatomic spacing and pseudopotentials chosen, which for now we assume are the same as in section 2, this model semiconductor's density of states has two energy bands (conduction and valence band) with a band gap of about 2 eV (see Figure 5). We assume the semiconductor eigenstates are unaffected by solvent motion, so that all V_o for the semiconductor are held constant. The electronic state of the redox species involved in the ET is assumed to not reach the valence band where electron exchange could also occur, i.e., we explore only conduction band processes in this paper. No solvent potential is used between the redox species and electrode.

1D Model of SLI Oxidation via a Conduction Band Process. *SLI Oxidation Behavior (Fixed V_o case).* We now investigate conduction band SLI oxidation with this simple 1D SLI model. For all 1D SLI oxidation studies we prepare the electron initially ($t = 0$) in the $n = 6$ eigenstate of the redox molecule. We take this state to approximate that for a redox species in equilibrium with the solvent, as in section 2. We denote the energy of this prepared redox species state as ϵ_{RET}. This state, of course, is actually quasi-stationary when the redox species is near the surface and energetically positioned in a band (see Appendix B). We now vary the magnitude of V_o, but hold it constant in time for any given run, since at the moment we want to study the "frozen solvent" regime. Figure 6 plots n_{REDOX} as a function of time under these conditions. Figure 6 shows that, as expected, no density is exchanged with the semiconductor when ϵ_{RET} lies in the band gap, i.e., n_{REDOX} is identically 1 for all times. When ϵ_{RET} lies in the conduction band, n_{REDOX} is zero in the long time limit, i.e., all the density escapes. Note the density in Figure 6 decays irreversibly and essentially exponentially in time in accord with well-known analytical models for the decay of a discrete state into a continuum of states.[5,17] Appendix B discusses how our ϵ_{RET} relates to the Gerischer model "energy levels".[16]

Our 1D models have revealed two well-known principles of quantum mechanics[5,18] which govern the behavior of our two systems. (1) When a discrete state $|\varphi_1\rangle$ is coupled to one other discrete state $|\varphi_2\rangle$, as in the homogeneous case, the system oscillates between the two states if resonance is set up (if the states are degenerate) and the potentials are time independent[5,18] (see Figure 3b). (2) In the SLI case where the discrete initial state is coupled to a continuum of final states, the system leaves the initial state *irreversibly* under the time independent potential conditions (see Figure 6).

These two fundamentally different behaviors also markedly affect the ET in the time dependent potential case, as we will see below. Irreversible behavior forms the foundations for many theories of solid-state charge-transfer reactions.[19−23] However the conceptualization, and the actual foundation, of many traditional theories used for SLI ET is exactly the oscillatory and discrete state picture of homogeneous theory.

SLI Oxidation Behavior (Time Dependent V_o). Of course, in SLI ET the potentials and electronic states are time dependent via their coupling to the solvent, semiconductor, and redox

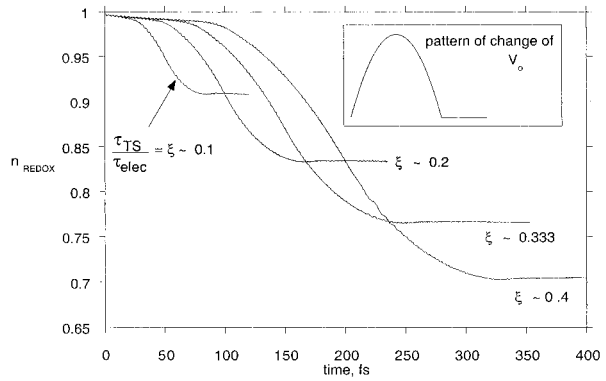

Figure 7. As the time spent by ϵ_{RET} in the conduction band (essentially the transition state lifetime, τ_{TS}) increases relative to the average lifetime of the redox species electronic state (τ_{EL}), n_{REDOX} decreases and P thus increases. We used eq 10 for this figure which makes ϵ_{RET} rise from the band gap into the conduction band and then drop back into the band gap, as the inset in the figure shows (recall ϵ_{RET} is essentially proportional to the V_o change).

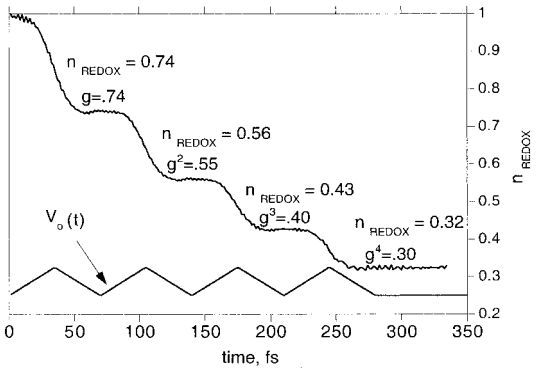

Figure 8. Multiple crossing of the band in the pattern shown in the figure, resulting in the n_{REDOX} shown (parameters are the same as in Figure 7 except the redox species is slightly closer to the surface). The quantities appearing are explained in the text.

species nuclear dynamics. In our 1D model during a solvent fluctuation to the heterogeneous oxidation TS ϵ_{RET} moves from a point near the reduced species average equilibrium position, which for simplicity we assume is in the band gap, to a position in the conduction band. For illustration, we implement this ϵ_{RET} movement via a simple time dependence for *all* of the redox species V_o (the same form as eq 8), and consequently also for ϵ_{RET}

$$\epsilon_{RET} \propto V_o = \hbar(\alpha(t - t_o)^2 + B) \qquad (10)$$

(if all redox species V_o change equally). This approximate proportionality was discussed for Figure 2. Use of eq 10 makes ϵ_{RET} rise from the band gap into the conduction band then drop back into the band gap as the inset in Figure 7 shows. This situation is obviously different than when this same time dependence is used for the homogeneous case (eq 8), since for the SLI case the electronic coupling is turned on the entire time the state is in the conduction band and the ET is characterized by irreversibility. The α in eq 10 is chosen so that the increase and decrease occur at a rate consistent with typical SLI solvent dynamics (we have investigated this elsewhere,[24,25] and we find so far that the transition state lifetime, τ_{TS}, can vary on average from about 10−1000 fs for various regimes and SLI systems). Figure 7 shows that as the time spent by ϵ_{RET} in the conduction band (essentially the transition state lifetime, τ_{TS}) increases relative to the approximate lifetime of the redox species electronic state (τ_{EL}) P increases (the long time n_{REDOX} decreases). This behavior can be interpreted via eq 11. Complete transfer can occur if $\tau_{TS} \gg \tau_{EL}$. Here, τ_{EL} depends, of course, on the redox species distance from the surface and its position in the conduction band (see appendix B).

The trajectory we considered here (band gap→conduction band→band gap) actually represents an unsuccessful nuclear trajectory for oxidation. A successful one would ultimately end up in the conduction band (our assumed equilibrium position of ϵ_{RET} for the oxidized species). For illustration purposes we are in effect making the simple assumption in our 1D models that there are only two distinct kinds of nuclear trajectories—one like that we described, and another that goes directly to product (from band gap to the equilibrium conduction band position of the oxidized species, and where total energy conservation would typically prohibit what would otherwise be complete ET). In a more realistic outlook, during each crossing into high coupling regions one can picture the trajectory as bifurcating as in surface hopping trajectory models,[9,26] as Appendix C discusses.

Figure 8 shows that in multiple crossings of a band of N states, n_{REDOX} decreases by a factor of approximately g for each full crossing. In Figure 6 we saw that in the case of static V_os the redox species electron density leaks out exponentially. Let us try to apply this to the dynamic V_o oxidation case by making the approximation that $g \sim \exp(-t_c/\tau)$, where t_c is the time to fully cross the band of N states once. If the electronic lifetime did not change appreciably as ϵ_{RET} varied, then τ would be a true measure of this lifetime, and one would obtain the approximate result

$$P \approx 1 - (1)\exp[-(\text{total time in band})/\tau] \approx 1 - [\exp(-N_C t_c/\tau)] = 1 - [\exp(-t_c/\tau)]^{NC} = 1 - g^{NC} \qquad (11)$$

where N_C is the total number of full crossings of this band. The last equality of eq 11 approximates the results of Figure 8 rather well (see Figure 8). In other model systems we find the match is not good primarily because the electronic lifetime can change significantly as ϵ_{RET} changes.

There will be reverse ET to the redox species from the same wave packet only by backscattering to the redox species via deviations from perfect crystal properties (defects, phonons, impurities etc.). Since these mechanisms typically would involve a significant energy change they would tend to be inefficient. In remaining discussions we will disregard these mechanisms unless otherwise noted.

1D Model for Reductive ET Process. We now examine reduction of redox species by electrons in the conduction band. This propagation of a bulk electron through a crystalline lattice with ultimate scattering into the surface and transfer to a redox species has no parallel in homogeneous ET. To better analyze the physics of this process, and for insight into SLI hot electron processes,[2] we will examine the effect of propagating electrons of various energies toward the surface.

In this section we explore the reductive regime by using the same 1D model and parameters as in the oxidative case. We use a Gaussian-type wave packet for the bulk semiconductor electron, which must of course be formed by a superposition of Bloch states. After the wave packet reaches a certain size the results are approximately the same, about the same as for plane waves. (The actual system specific size can be estimated from the Heisenberg uncertainty relation, $\Delta x \sim 1/\Delta k$, where

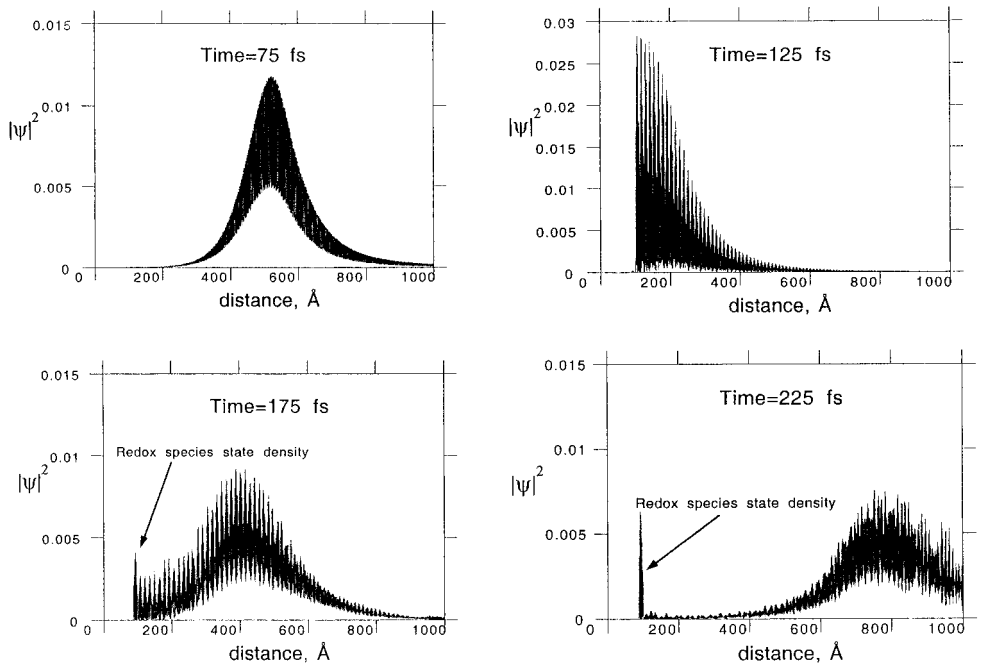

Figure 9. Wave packet propagating toward the redox species for one particular semiconductor electron energy. Part of the incident density is transmitted and part is reflected. Part is captured transiently in the redox species, as noted in the figure.

Δk is chosen to be representative of wavenumbers for conduction band semiconductor electrons.) We employ these large wave packets below.

SLI Reduction (Fixed V_o Case). We now study the effect of varying the energy of the electron impinging on the surface, while holding *all* V_o constant in time (fixed solvent regime). We again arbitrarily choose the $n = 6$ eigenstate for ET and position ϵ_{RET} at about 0.03 eV above the conduction band edge by using a particular V_o (recall we assume the oxidized species' equilibrium ϵ_{RET} is in the conduction band and the equilibrium reduced species' ϵ_{RET} is in the gap). We then choose electrons of various initial total energies, of a given wave packet size, and with a given initial group velocity (we use a typical thermal velocity of 1.e7 cm/s [27−29]). We do not use an applied potential. Figure 9 shows the wave packet propagating toward the redox species for one particular electron energy near resonance. Figure 9 shows that part of the incident wave is transmitted and part is reflected, which is of course familiar quantum behavior. The most interesting behavior for purposes of ET is that a quasi-stationary state of the redox species transiently traps some of the electron density which then leaks back into the semiconductor after a time delay, i.e., reemission occurs (see Figure 9). This is also familiar quantum behavior.[5,17] If this transient density on the redox species can be trapped, e.g., by the solvent by causing ϵ_{RET} to fall into the band gap, then reduced redox species product can be formed. For ease of exposition we will focus on the exact kind of successful nuclear trajectory just mentioned; other scenarios are analogous. The occupation plots discussed next portray the behavior just described.

Figure 10 plots n_{REDOX} as a function of time for various initial electron energies, keeping all V_o fixed, as in the last paragraph. This figure shows that the redox species is filled to various maximum occupation values in varying amounts of time as a function of the various semiconductor electron energies. Note in Figure 10 the rapid change in lifetime of the redox species state, as measured by its decay from the peak of the occupation profile, with electron energy. This sensitivity to electron energy, of course, is the hallmark of resonant behavior.[5,18] We get a

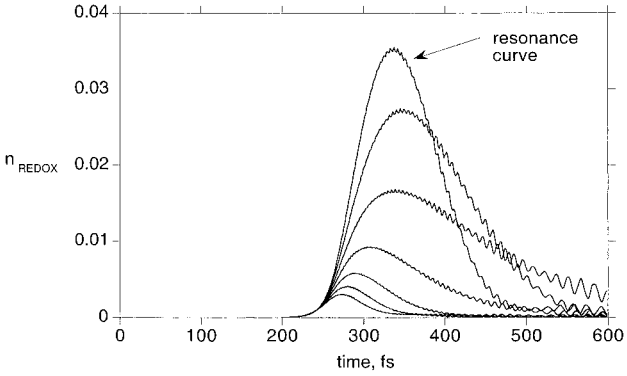

Figure 10. Plot of n_{REDOX} as a function of time for various initial semiconductor electron energies (over a range around the resonance energy of about ±0.025 eV).

peak in n_{REDOX} near electron energies of about −8.8 eV, as one would expect for resonant scattering into the $n = 6$ eigenstate for $V_o \sim -20.0$ eV. On resonance, both the wave function in the redox species and the decay lifetime match that of the $n = 6$ eigenstate. This indeed shows the state occupied by the electron is a quasi-stationary state related to the $n = 6$ eigenstate. Off resonance, the occupation curves can of course show more complicated behavior than symmetric filling and decay (see Figure 10). Very similar n_{REDOX} behavior to that just discussed occurs in our model for electrons of given energies scattering into redox species having different ϵ_{RET} caused by solvent configuration differences (different redox species V_os in the 1D model).

Reduction (Time Dependent V_o). Let us briefly examine the effects of solvent dynamics on SLI reduction by introducing a time varying V_o. In Figure 11 we plot n_{REDOX} as a function of time assuming that all the redox species V_os change linearly in time, forcing ϵ_{RET} to change from the average value of the oxidized ϵ_{RET} (situated in the band) to a value in the band gap (to the average reduced ϵ_{RET} value). The rate of change chosen is consistent with solvent dynamics. We vary the electron impact time, as noted in the caption for Figure 11, by starting the electron wave packet propagating at different times relative to

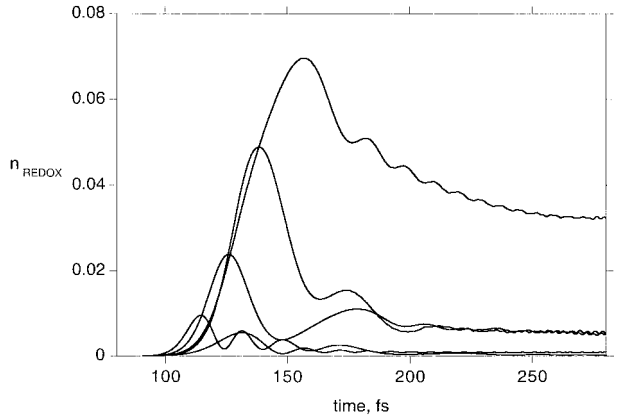

Figure 11. Plot of n_{REDOX} as a function of time assuming that all the oxidized redox species V_o simply decrease linearly in time over values described in the text. All V_o for the semiconductor are held constant. The incidence time of the wave packet varies over about a 200 fs range.

the time V_o is started changing from its equilibrium value (propagation distance is fixed). Figure 11 shows that there is complicated interplay between the ϵ_{RET} dynamics and the electron dynamics. That is, to capture significant density we must have ϵ_{RET} near the resonant energy when the electron wave front is close enough to the surface to allow tunneling. Figure 11 shows again (as in Figure 10) that the density in the redox species reaches a maximum, after which time density is "reemitted" back into the semiconductor, but the sinking of ϵ_{RET} into the band gap can now stop the reemission process. If the redox species is close to the surface, the emptying time back into the semiconductor will be short (via $\tau_{EL} \sim \hbar/|V|$) and the solvent must bring the level quickly into the band gap to trap significant density. If it is far from the surface, the emptying will be slow (as will the filling on resonance). Thus in this picture for a given rate of change of V_o there can be an optimal distance where the trapped density in the redox species is highest.

Other Regimes of SLI ET. Up to now we have been talking about standard SLI ET. But our model is also applicable to surface state and adsorption mediated SLI ET, photoexcited SLI ET, defect mediated SLI ET, and other related ET scenarios. We give an overview of these applications in the Supporting Information Appendix S.2.

IV. SLI ET − Three-Dimensional WPMD Models

We now very briefly explore three-dimensional (3D) SLI WPMD models; a complete investigation is reserved for another paper[30] in which we report interesting results for 2D models as well. We will see that the 1D model captures important qualitative physics of the 3D systems.

Our WPMD simulations are fully dynamic 3D simulations addressing the ET electron, solvent, redox species, and semiconductor using realistic pseudopotentials for all atoms. The one-electron 3D WPMD that we discuss here is an extension of traditional MD. Many traditional (fully classical) MD simulations use pseudopotentials of the form we employ for WPMD. But traditional MD (TMD) can only account for the electron in the most primitive of fashions. The fundamental difference between TMD and WPMD is that the ET electron is treated quantum mechanically by using the time dependent Schrödinger equation. We use several different variations of WPMD described in Appendix C. One is analogous to the frozen solvent approximation above. Another simply uses fully classical nuclear MD trajectories and is thus similar to the approach of LZ theory and our 1D fixed trajectory models. In the third version the interatomic forces in our WPMD have fixed distance dependencies (Coulomb and short range forces) like TMD, except for those significantly influenced by the changing ET electron density. This final version thus addresses the self-consistent coupling between the nuclear and electronic dynamics. One can easily see the form of WPMD we use here is conceptually a straightforward extension of the 1D model discussed above; the primary differences (besides dimensionality) are that the solvent, redox species, and semiconductor interaction and dynamics are explicitly included and electron density can penetrate the solvent. We describe details of our WPMD in Appendices C and S.1.

The solvent chosen for the simulations below is the SPC model of water.[24,31−33] The redox species model uses pseudopotentials of a general form for molecular species consisting of octahedral waters centered on a transition metal. We examined two redox species systems with these kinds of pseudopotentials. One was the ferrous−ferric redox species system in all details but one. Namely, we used all the same pseudopotential parameters used in numerous other ferrous−ferric studies,[24,31−33] except we modified, in effect, the ionization potential to give qualitatively the same energetics as discussed with our 1D models (see Appendix S.3). The second redox species was exactly the same as that just described except we used a different electron−ligand (water ligand) pseudopotential, as discussed in Appendix S.3. The main intention of this last design was to trap electron density in a more delocalized fashion than the ferrous/ferric system (interesting physics of this system will be reported elsewhere). Semiconductor electronic structure can be described in great detail with pseudopotentials. But here we used only local pseudopotentials representing (100) GaAs. See Appendices C and S.1 for further detail.

With this background we now introduce results from 3D one-electron SLI ET WPMD simulations. To our knowledge these represent the first SLI simulations using such methods.

In Figure 12 we show the results of propagating an electron wave packet from the semiconductor bulk to the surface in a fixed trajectory WPMD simulation using the second redox species described above (which traps significant density on each of its six "oxygen" atoms, see Appendix S.3). The solvent configurations involved are TS configurations where the total system energy for the ET was conserved (within a tolerance achieved using techniques discussed in Appendix C) when ϵ_{RET} lay in the conduction band. This figure reflects much of the important physics seen in the 1D model. One can see (see figure caption) that part of the incident wave packet is transmitted to the redox species and part is reflected back to the bulk. A quasi-stationary state of the redox species (note some of its atoms become outlined with density) transiently traps some of the electron density which then leaks back into the semiconductor after a time delay, i.e., reemission occurs. Some penetration of density into the solvent can be seen, which is short lived. The effect of solvent dynamics is of course very important in the ET, and we briefly examine it next.

A 1D SLI ET model cannot quantitatively match a 3D model, but the 1D model does capture many of the central qualitative trends of the 3D case. If we examine n_{REDOX} from representative times in the fully dynamic 3D SLI ET simulation, we obtain results similar to the 1D case. For example, for the reduction process we again have a quasi-stationary redox species state forming from electron injection with the same sensitivity to electron energy as we saw in Figure 10 above. Also, n_{REDOX}

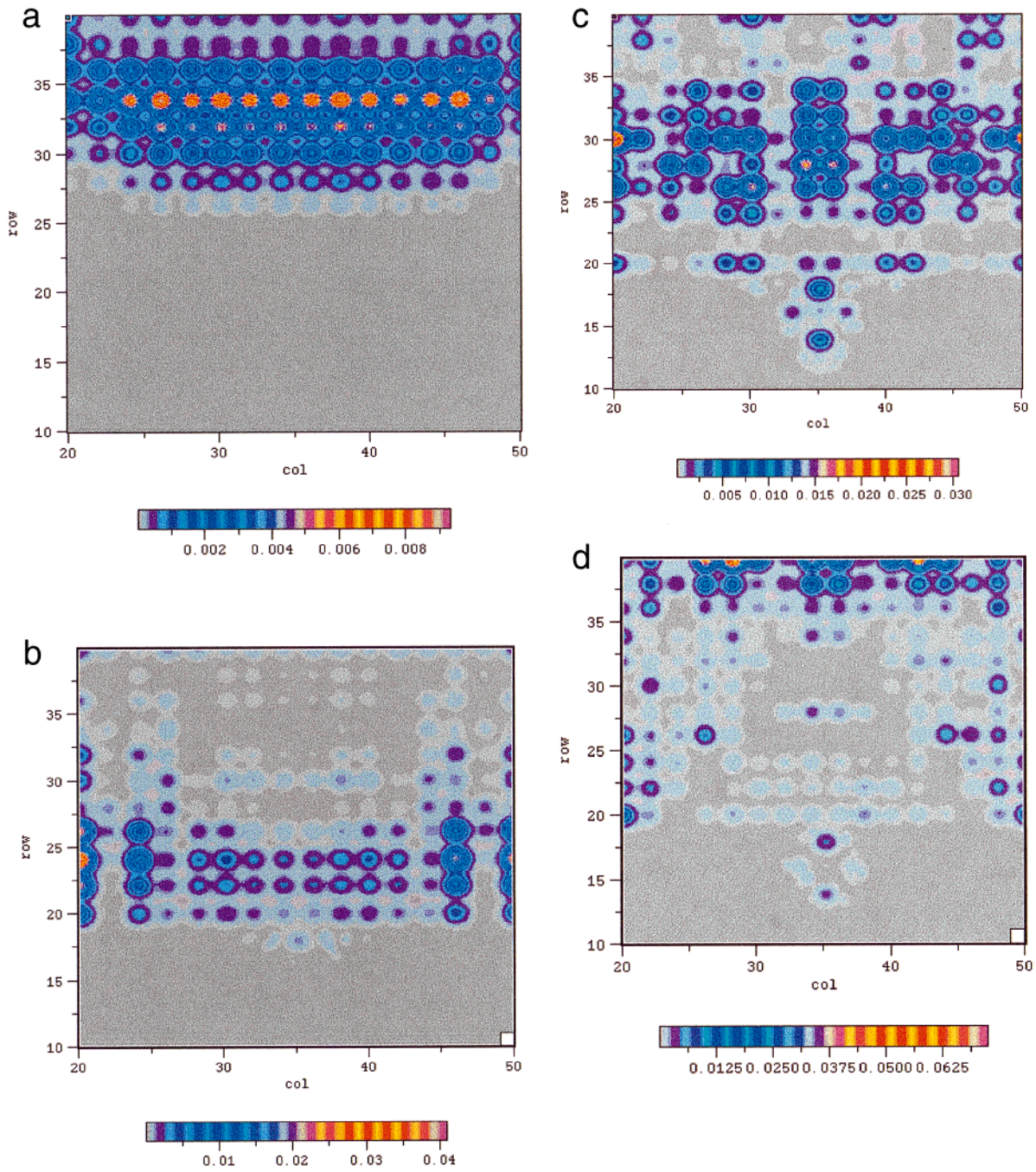

Figure 12. 3D results of propagating an electron from the semiconductor bulk to the surface with a fixed trajectory WPMD simulation using the second redox system in the text. The various frames show successively longer times. The figure is a contour plot (2D slice perpendicular to the surface). Orange is the highest electron density, blue-green shades are less, and gray is least (see key). Note the center of the semiconductor surface atoms are at about 20 Å on the vertical "row" scale ("col" scale is also in Å). The wave packet initially approaches the semiconductor surface. Some lattice atoms of the (100) GaAs semiconductor are outlined by density. The particular 2D slice we used, and the coarseness of grid we employed, does not well resolve the density, but it does well illustrate the trends discussed in the text. The redox species was held fixed in an "apex toward surface" position at a orientation such that four ligand atoms' densities appear. The total elapsed time was about 300 fs.

versus time results from fixed or self-consistent trajectory 3D WPMD simulations often resemble the plots in Figure 11 (e.g., see Figure 13 which used the first redox system just discussed above).

We will present detailed results of 3D WPMD simulations in another paper[30] including those for typical SLI systems (we are currently refining acetonitrile pseudopotentials and pseudopotentials for redox species used in that solvent). For now, we summarize our results by saying that while the qualitative results of one and higher dimensional models are similar, there are also significant differences. For example, studies of one-, two-, and three-dimensional systems regarding Anderson localization have proven that electron localization is highly dependent on dimension.[34] This can have important effects in disordered systems,[34] and there can be appreciable disorder in the solvent and semiconductor interfacial region. Also, near-surface solvent can play a significant role in the scattering process. In a 1D model the latter effects are simply not addressable for obvious reasons. The quantitative results of higher dimensions, as one would expect, are very different; one simply cannot even describe the molecules we chose in this section with a 1D approach.

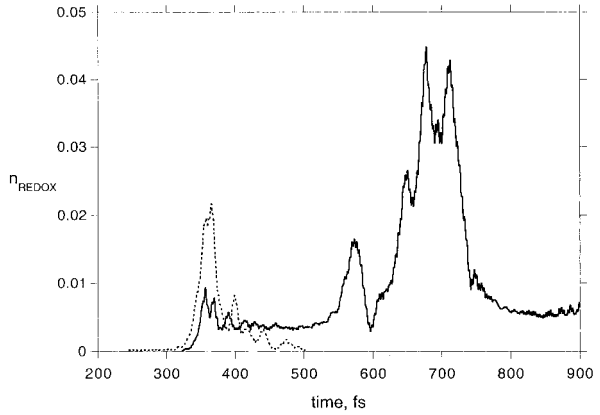

Figure 13. Plot of n_{REDOX} as a function of time for a fixed nuclear trajectory WPMD simulation for the first redox system of the text. The dashed curve is quite similar to some of those in Figure 11. The solid curve is a prolonged excursion in the TS, which one can see ultimately results in trapped density. It too has features similar to Figure 11. As Appendix E discusses, the ionization potential of the ferrous/ferric system was adjusted to qualitatively match the energetics of the 1D system of the text.

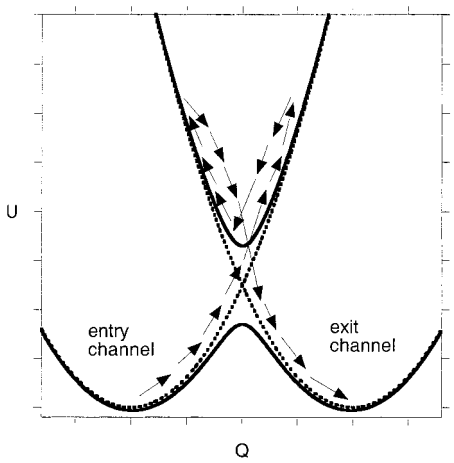

Figure 14. (Free) energy curves of the two-state model, familiar from quantum mechanics textbooks, and ET theory. Both diabatic (dashed) and adiabatic (solid) curves are shown. Also shown are pathways to determine P for the normal regime homogeneous system. These trajectories consist of a nonadiabatic ascent to the upper energy surface, an odd number of "adiabatic" oscillations in the upper well, with a final nonadiabatic descent into the reactant well. There is also a purely adiabatic pathway (not indicated).

V. Discussion and Further Development

Above we overviewed homogeneous and SLI ET from the perspective of our wave packet methods and discussed connections to LZ theory. We now revisit these issues by introducing additional models. This will serve to relate our wave packet approaches to traditional and modern ET theory in more detail, and to point out important implications.

Features of the LZ Model Relevant to SLI ET. So far we have not examined multiple crossings in the high coupling region in any detail. In this section we examine this via LZ theory using its reaction coordinate formulation (see appendix A) rather than time dependent eigenstates. In this language then, the high coupling regions are the diabatic intersections where in an adiabatic representation the avoided crossing splitting arises (see Figure 14). We saw that only two eigenstates are considered in the LZ model, rather than a discrete eigenstate coupled to multiple states, as we have been discussing for the SLI case. We here extend the original (unmodified for QI) LZ model to the multistate SLI ET case in the most straightforward manner possible.

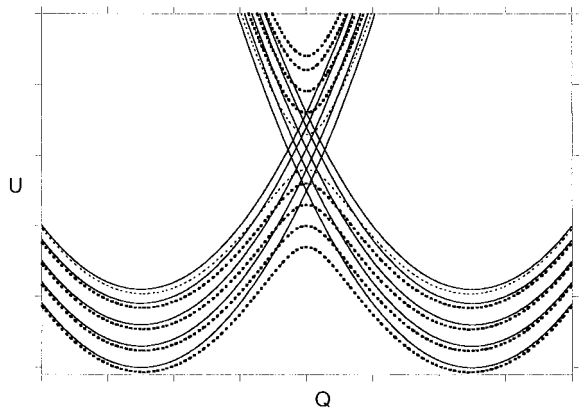

Figure 15. Manifold of reactant (R) and product (P) curves assumed in traditional theories of electrochemical ET. These R and P curves are assumed to differ only in the distribution of the solid's electrons among the solid's eigenstates so that the solvent contribution to each curve is identical (the dependence on the solvent coordinate, Q, is identical for each curve).

LZ theory essentially assumes a probability associated with a trajectory as contrasted with a transition amplitude associated with a wave function. We will speak freely of probabilities, as opposed to transition probabilities, in association with it.

Homogeneous κ. In traditional homogeneous ET theory the overall ET κ (that used in eq 9) is regarded as the sum of the probabilities of product production by various pathways through the intersection region of the two-state model. In the normal ET regime[4,14] these pathways/trajectories consist of ascent along the initial diabatic curve to the upper energy surface, an odd number of "adiabatic" oscillations in the upper well, with a final nonadiabatic exit from the upper surface and into the reactant well (see Figure 14). There is also a purely adiabatic pathway along the lower surface. Within the two-state LZ model p and $(1 - p)$ are the probability of these nonadiabatic and adiabatic crossing events. Thus the infinite sum which gives the normal regime homogeneous P is[14,35]

$$\begin{aligned} \mathrm{P} &= (1-p) + p(1-p)p + p(1-p)(1-p)(1-p)p + \ldots \\ &= (1-p) + p^2 \sum_{j=0}^{j=\infty} (1-p)^{2j+1} = 2pp/(1+pp) = \kappa_{\mathrm{LZ}} = \kappa \end{aligned} \tag{12}$$

where $pp = 1 - p$.

In the inverted ET regime there are only two pathways which give[14,35]

$$\mathrm{P} = p(1-p) + (1-p)p = 2p(1-p) = 2pp(1-pp) = \kappa_{\mathrm{LZ}} = \kappa \tag{13}$$

Eqs 12 and 13 are typically used for κ in eq 9 in both homogeneous and heterogeneous ET. (The parameters of p (see eq A.2) in eqs 12 and 13 in this ET context are given in eq A.3.) But this practice is highly problematic for the heterogeneous case, as we now discuss.

LZ Theory for Solid-State Systems. When the continuum of states in the electrode is addressed in traditional theory, it is usually assumed to result in the situation portrayed in Figure 15. The manifold of reactant (R) and product (P) curves in Figure 15 is obviously a simple extension of the two-state model in Figure 14. These R and P curves are assumed to differ only in the distribution of the solid's electrons among the solid's

eigenstates,[11,36] so that the solvent contribution to each curve is identical. The lowest R curve in Figure 15 is assumed to contain energetic contributions only from the ground state of the solid's electronic system (all states below the Fermi energy are filled).

It has been stated that no analogue of the LZ model has been published for the manifold in Figure 15.[4,11,37] We derive such an analogue model here, with details given in Appendices D and S.4. We explore this topic because it is still perhaps the predominant electrochemical mental picture in the literature, and it will contrast perspectives of our WPMD approach with traditional models and highlight some fundamental shortcomings of the latter.

We pause to note that we did not explicitly consider the solid's electron configuration above. The subject of solid-state excitations in our opinion requires a more rigorous approach than suggested by the manifold in Figure 15. Excitations could be addressed in our WPMD model in any of a number of well-known ways,[23,27,29,38−42] but it is unnecessary for our purposes and would greatly complicate matters (see ref 13). Below we address the full manifold of curves in Figure 15 not because of any direct interest in excitations per se, but because the conclusions we will reach point out difficulties with the LZ approach to a multistate system.

We assume in this section that the probability, P, of reduction or oxidation from a one-electron level follows, respectively, the traditional formulas[11]

$$P \sim n(\epsilon)f(\epsilon)\exp(\epsilon/2kT)$$
$$P \sim n(\epsilon)(1 - f(\epsilon))\exp(\epsilon/2kT) \quad (14)$$

where f is the Fermi−Dirac distribution function, $n(\epsilon)$ is the solid's DOS (typically assumed a constant in traditional theory), and $\exp(\epsilon/2kT)$ is the activation energy term. Both expressions are, approximately, peaked around a maximum at the electrons' electrochemical potential in the solid.[11] The two expressions in eq 14 have significant magnitude only over a few kT, so we assume there is negligible change in the activation energy in reaching the various intersection points in Figure 15. These are the assumptions typically used in traditional theory,[4,11] and they greatly simplify expressions below.

To develop our multistate generalization of LZ theory, which we will call M-LZ theory, we employ the original LZ model and thus assume that crossings at each intersection are independent, i.e., no quantum coherence/interference occurs. Then, for example, the probability of moving along any R curve in Figure 15 to the classical turning point above the uppermost P curve is just the product of probabilities of the independent crossing events

$$p_M = p_1p_2p_3p_4\cdots p_N = \prod_i p_i \quad (15)$$

where p_i is the LZ two-state model probability (eq 6) for each of the curves' intersections (see Figure 15) for N states/curves. We call this probability p_M (denoting p multistate) because in the two-state model the analogous pathway would have probability p. Matters are simplified if we set all p_i in eq 15 to a given value p_o. Thus for now we assume

$$p_M = p_o^N \quad (16)$$

We now examine the LZ probabilities for the multistate system of Figure 15 by employing eqs 15 and 16. In Figure 16

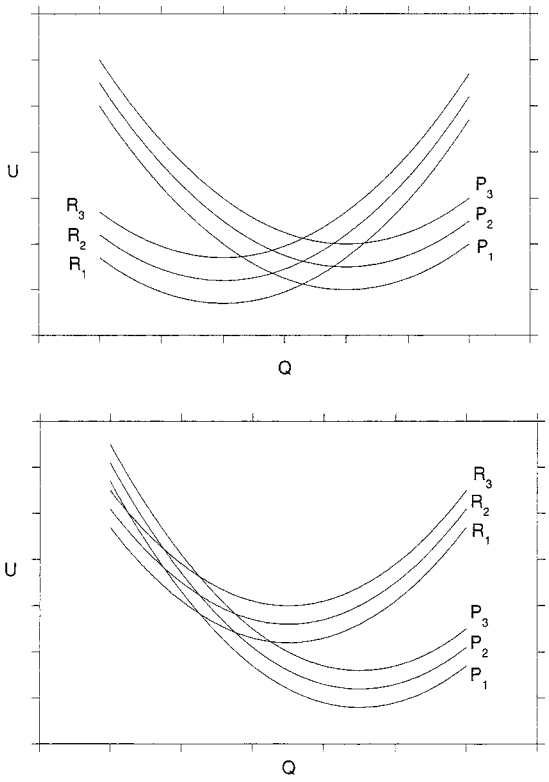

Figure 16. We label the normal (a) and inverted (b) ET regime curves from $j = 1$ to $j = N$ for the R and P curves from the lowest to highest curve respectively (only three curves are shown for illustration).

we have labeled the inverted and normal ET regime curves from $j = 1$ to $j = N$ for the R and P curves, from the lowest to highest curve, respectively (only three curves are shown for illustration). Under these conditions the LZ probability, $P(R_j \Rightarrow P_i)$, for going from an arbitrary curve R_j in Figure 16 to any of the product curves, is easily calculated, as Appendix D shows. In both the normal and inverted regimes for large N we find that approximately

$$P(R_j \Rightarrow P_i) \sim p_o^{j-1}(1 - p_M N_F) \quad (17)$$

(large N limit, normal + inverted regimes), where N_F is the number of full crossings of a band composed of N states. (There are order N "subcrossings" in every full crossing (see Appendix D).) All lateral crossings for every curve j above $j = 1$ are accounted for by the p_o^{j-1} term of eq 17 (see Appendix D). We are obviously assuming, for now, that every full crossing involves the same N states. The primary reason for the approximate inverted and normal regime equivalence (exhibited by eq 17) is that there is effectively a "pure adiabatic" pathway ($1 - p_M$ pathway) in both regimes in the multistate case, and this pathway contributes most to P (see appendix D). For smaller N significant differences arise in the two regimes, especially for $N = 1$ where the expressions in Appendix D reduce to the two-state equations (eqs 12 and 13).

N_F is restricted to an upper limit of a relatively small integer number (see Appendix S.4). This, fortuitously, is in accord with SLI simulations we have reported elsewhere,[24,25] but the states involved typically vary from one full crossing to the next, so that our "same states" assumption is highly idealized. The number of states N considered in eq 17 are only those in a small energy range $\Delta\epsilon$ involved in the TS crossings (via eq 14).

Note that for all low j curves ($j \sim 1$) we obtain ($p_o \sim 1$, even for very small p_M since $p_M = p_o^N$ and N is large)

$$P(R_1 \rightrightarrows P_j) \sim (1 - p_M N_F) \tag{18}$$

(small j, large N limit). This is the same qualitative behavior that our 1D model exhibits under ideal conditions (see eq 11). We will see later that this apparent match (eq 11 and eq 18) between M-LZ and our wave packet results is largely fortuitous, and also that M-LZ fails for more realistic models.

In LZ theory $|V|$ is a parameter describing the electronic coupling and thus the splitting between the energy surfaces. But the total energy spacing between the splittings (see Figures 15 and 16) is unaccounted for in the M-LZ model. Indeed for a given $|V|$ and α (see eqs 6, 16, 17, and Appendix D) only the *number* of curves/states N affects P in the M-LZ model. Thus a peculiarity of the M-LZ model is that the entire band of N given curves can be assumed to encompass an arbitrarily small or large energy interval and no change in P occurs. This is a consequence of the semiclassical nature of LZ theory and its two-state foundations. As we will see in the TDAN subsection, a quantum model shows important dependencies on this spacing and the structure of the electronic DOS.

From what we just discussed it is obvious that the M-LZ model essentially disregards the electronic DOS (number of states per unit energy is neglected). Thus it is not possible to develop M-LZ expressions for P which are properly weighted by the DOS of the solid, or show any other DOS effects. The DOS, of course, plays a crucial role in models of charge transfer in the solid state (see refs 19−21 and Appendix E). Regarding weighting, we include only that which arises from the Fermi−Dirac distribution function. Via this distribution one expects the lowest R curves to be most populated and higher energy curves less populated. We can write an expression for the total probability of ET from the entire family of curves R_j to the entire family of curves P_i in terms of these relative populations as

$$\kappa = P_{TOTAL} = \sum_{j=1}^{j=N} W_j[P_j(R_j \rightrightarrows P_i)] \tag{19}$$

where W_j is the relative population of reactant curve R_j; $P_j \leq 1$ for all j, and $\Sigma_j W_j = 1$.

Equation 19 is our M-LZ model's expression for the total probability of the electronic system moving from R to P curves given that the TS region has been reached. By definition then, eq 19 is the κ to be used in eq 9 for the rate constant within the M-LZ framework (recall we deal only with the local rate constant in this paper;[15] there is a different κ for each separation distance from the electrode). Obviously this expression (eq 19) neglects redistribution from product minima to reactant curves (this is the back reaction). We also neglect back reaction/redistribution to other reactant curves "in route" to product. Appendix S.4 discusses these pathways.

In the limit in which the two bands of R and P curves in Figures 15 and 16 become infinitely thin (in energy spacing), one expects the two-state model and the multistate to match (a set of nearly degenerate solid-state eigenstates will exist if the bandwidth is very small). If there is to be any hope of matching we must construct our M-LZ model so that $p = p_M = p_o^N$; then we must have via eq 6, 7, 15, 16, and A.2

$$p_M = p_o^N = \prod_{k=1}^{N} \exp[-(2\pi(|V|^2/N))/(\upsilon \Delta F)] = \exp[-2\pi|V|^2/(\upsilon \Delta F)] = p \tag{20}$$

where υ and ΔF are the familiar LZ parameters defined in Appendix A. To form the equalities shown in eq 20, a number of very restrictive approximations must hold (see Appendix D). Equations of the same form as eq 20 have been utilized in the solid-state literature.[22,23,43]

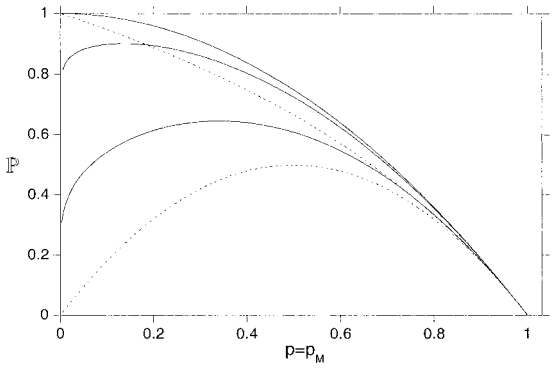

Figure 17. Results from eq 19 for P using Fermi−Dirac weighting. The solid lines are heterogeneous results. Over the typical range where P for the oxidative case of eq 14 is appreciable (a few kT were assumed for this figure) the Fermi−Dirac distribution, f, spans a range near 0 to nearly 1. Depending on where this distribution is centered within the N states considered in the M-LZ model, very different results are obtained, since the upper or lower j curves can dominate P. The solid curve that approaches 0.8 as $p_M \rightarrow 0$ had f centered in the "band gap" (below the lowest state in energy) and gave significant weight to lower curves. The other curve had a center closer to the bottom ($N = 1$) state and gave more weight to upper R curves. The top solid curve is $1 - p_M^2$. The curves plotted assumes $N_F = 2$ and that $N = 60$. The dashed curves plot the homogeneous P (eqs 12 and 13).

Using eq 20 we can plot the results of the two-state and M-LZ κ on a common axis, i.e., κ vs $p = p_M$. If we employ eq 14, then over the typical range where the exponential term is appreciable (a few kT) the Fermi−Dirac distribution, f, spans a range near zero to nearly 1. With this weighting the upper j curves can play a significant role depending on where f is centered relative to the N states considered (see Figure 17). If they do play a significant role then in the normal regime, P is always less than 1 as $p = p_M \rightarrow 0$ (for large j and large N eq 17 is approximately $p_M(1 - p_M^{N_F})$). This is qualitatively different behavior than for κ in the two-state normal regime (see eq 12). In the inverted regime, if upper j curves are important, κ versus p and p_M curves are qualitatively the same for the two and multistate cases (see eq 13). All this κ behavior is very sensitive to the weighting, and the weighting we suggest is obviously quite approximate. If lower states were the biggest contributors to κ, then the qualitative differences are reversed (biggest for the inverted regime). Figure 17 shows some results from eq 19. Since energy separation between states is essentially a foreign concept to the M-LZ model, weighting the N states with the Fermi−Dirac distribution is itself problematic. These qualitative discrepancies and anomalies are one reason that the practice of using the two-state κ result (eqs 12 and 13) for multistate ET systems appears highly questionable. Large *quantitative* discrepancies also arise for $N_F = 2$ and higher ($N_F = 2$ was assumed in Figure 17).

Other serious problems arise if more realistic multistate models are employed. We assumed above that $p = p_M = p_o^N$

for *every* curve R, and that therefore (via eq 20) the coupling for *every* intersection is the same. But the electronic coupling matrix elements, $|V|$, at each intersection (see Figures 15 and 16) and other LZ parameters for arbitrary R and P curves are significantly different for more realistic models (e.g., even our 1D model, recall the discussion of Figures 6−8). Thus, the p_i (see eq 15) vary nonuniformly. In this case eq 15 shows that p_M will be different for every curve R_j. In short, the coupling and pathways in the multistate LZ system are much more complicated than in the two-state system. The drawing of analogies between the two systems, either conceptual or mathematical, can become impractical and finally impossible with sufficient deviations in $|V|$ at each intersection.

The "full crossings" we spoke of above are an idealization, as noted above. In the simulations we have reported elsewhere[24,25] the trajectory has a random path through the band during the TS lifetime. So the same N states are not covered in each of multiple crossing events, and a situation akin to the random matrix elements problem arises also for this reason.

We have so far seen there are two basic problems with the LZ approach. First, it is highly problematic to apply the two-state κ equations (eqs 12 and 13) to a multistate system, even to our simple M-LZ model system. Second, the M-LZ model itself has fundamental problems. At *extremely* low coupling ($p = p_M \rightarrow 1$) all models considered herein tend to converge to the same answer for κ, i.e., the Fermi Golden Rule limit (the $p = p_M \rightarrow 1$ limit of figures above). However it is highly unlikely that the coupling is universally this weak in these systems.[1,24,25] Certainly it cannot be for adsorbed systems, and we have calculated that the coupling is relatively high in other SLI systems as well.[24,25]

TDAN Model. In this section we introduce a model Hamiltonian approach to the multistate curve crossing problem. This serves to point out the relation of our WPMD model to modern heterogeneous ET theory and to further elucidate LZ difficulties.

Time dependent model Hamiltonians for multistate electronic systems have been addressed extensively in solid-state literature. These are typically applied to charge transfer to/from atoms or molecules colliding with solid surfaces.[19,22,23] The model Hamiltonian we will use for discussion here is a spin independent, time *dependent* Anderson−Newns (TDAN) Hamiltonian with a boson term.[22,23,44,45] We write this Hamiltonian as

$$H_e = (\epsilon_{eff}(t))c^\dagger_a c_a + \sum_k \{\epsilon_k c^\dagger_k c_k + (V_{ak}(t)c^\dagger_a c_k + V_{ka}(t)c^\dagger_k c_a)\} + \sum_i \hbar\omega_i(b^\dagger_i b_i + 1/2) + \sum_i \eta_i \hbar\omega_i(b^\dagger_i + b_i)(z - c^\dagger_a c_a) \quad (21)$$

Hamiltonians such as eq 21 are applicable to SLI and metal−liquid ET, and the time *independent* version of it has been adapted to both.[24,25,46,47] The time dependent solution, which we discuss now and in Appendix E, has not previously appeared in the solid−liquid ET literature to our knowledge. Here, $c^\dagger_i(c_i)$ are the creation (annihilation) operators for the single electronic state of the redox species considered (i = a) and for the solid states (i = k); z is the oxidized ion charge; and η_i is discussed later and in Appendix E.

To employ eq 21 for our SLI system we assume

$$\epsilon_{eff}(t) = \Delta E(t) + \epsilon_a \quad (22)$$

where ϵ_{eff} is the eigenvalue of the eigenstate to and from which the ET electron transfers and ϵ_a is a chosen reference energy level.[13] ϵ_{eff} is directly analogous to the ET state, ϵ_{RET}, in our models in sections 3 and 4. However we assume in the TDAN model that ϵ_{eff} is a single s-like orbital, since this allows eq E.1 to be easily solved.[22,23]

ΔE in eq 22 is the difference in the energy of interaction of the redox species (oxidized and reduced forms) with a fixed solvent and semiconductor nuclear configuration present at an instant in time. ΔE is thus directly analogous to the solvent coordinate used widely in modern homogeneous ET theory, and we have discussed its meaning in the current context at length.[24,25] Equation 22 is a highly approximate model for the dependence of ϵ_{eff} with solvent configuration, which obviously assumes ϵ_{eff} changes additively with the Coulombic and short-range interactions comprising ΔE. We have discussed the time independent version of eq 22,[24,25] to which eq 22 is directly analogous, in detail.[24,25,48] ΔE can be calculated directly from the WPMD simulation, in standard ways.[13,24,25,32,49,50]

The eigenstates in the solid are labeled ϵ_k in eq 21, and these correspond, for example, to the eigenstates of our pseudopotential semiconductor model and they collectively form the semiconductor DOS. We will discuss the meaning of the boson term (the second line of eq 21 containing the boson operators (b_i)) near the end of this subsection.

Let us first omit the boson term in eq 21, and examine the remaining Hamiltonian. So that we can compare to the LZ model, we assume the electronic coupling is independent of time (except for a rather trivial turning on and off when the band gap is reached), and thus V_{ak} and V_{ka} in eq 21 will be constants. The only time dependence which then remains in the Hamiltonian is that of the redox species eigenvalue, ϵ_{eff}. For example, we can use the same form as eq 10 for $\Delta E(t)$, so that $\epsilon_{eff}(t)$ varies parabolically in time via eq 22. The important point is that the solvent is assumed to have a fixed trajectory. Thus, for now, we make the same assumptions as in our 1D models above and in the LZ model. We are also assuming the electronic coupling is energy independent. The explicit way we do this in the TDAN model is discussed in Appendix E.

With these simplifying assumptions the time dependent Schrödinger equation using the Hamiltonian, eq 21, can be easily solved, as shown in Appendix E. An expression for P can be derived directly from results in the solid-state literature.[22,23] P is simply $n_{REDOX}(t \rightarrow \infty)$ of eq E.12, where this long time limit has the same meaning as in section 2, and multiple crossings can be addressed. The more general case of time dependent electronic coupling and ϵ_{eff} can also be addressed by the TDAN model in Appendix E.

TDAN Discussion. The TDAN model and our WPMD method can be used to describe a number of important features of the discrete-continuum ET system for which the LZ theory gives anomalous results.

One of these effects is associated with the inverted region results above (eqs 13 and 17). In the inverted regime the M-LZ model gives, for two full crossings, approximately $1 - p_M^2 = 1 - p^2$ for P for the small j curves (see eq 18) rather than the qualitatively different two-state result ($2p(1 - p)$, eq 13). M-LZ predicts this same result regardless of bandwidth, since it effectively ignores energy spacing. This is an erroneous prediction because as the bandwidth becomes very small a multistate system should behave like a two-state one (again, a set of nearly degenerate solid-state eigenstates will exist if the bandwidth is very small). These kind of anomalies have been discussed elsewhere.[45]

In contrast, TDAN and our WPMD model both give appropriate results because both models accurately address the DOS of the solid and QI effects so they show reversible versus

irreversible behavior for narrow versus wide bands, respectively. Therefore in the inverted regime one qualitatively sees $P \sim 2p_M(1 - p_M)$ behavior for very narrow bands (such as eq 13), versus $P \sim 1 - p_M^{N_F}$ for wide bands (see eq 18). Tsukada has explored these topics for the TDAN model (eqs E.1−E.12).[22,23] We show in more detail in Appendix S.5 the behavior of our model in narrow and wide band limits. Since the results we have just described depend sensitively on the DOS, M-LZ theory is unable to address them.

It is easy to demonstrate that we expect M-LZ anomalies such as those we have just discussed and that M-LZ theory thus disregards essential physics of problems such as SLI ET. Let us reexamine the fundamental LZ equations (eqs 5, 6, and 7). There are only two adjustable parameters in eqs 6 and 7, α and $|V|$ where α simply describes how fast the diabatic eigenvalues change with time, and it is a fixed quantity. $|V|$ describes the splitting between the energy surfaces, but the spacing *between* splittings is not described, as we saw above. As a consequence, crossing a narrow band is the same for M-LZ theory as crossing a wide one if we assume equal $|V|$ and N for the two bands. But, for a given α, if the band is narrow in energy there will be less time spent in it than if it is wide, and less time spent in the high coupling regions. There is no way to account for this in M-LZ other than by changing $|V|$ in an arbitrary and physically meaningless way or by introducing physically unsound ad hoc parameters to modify α. But such an accounting is essential for, as we saw in section 3, one of the key effects is the length of time the eigenstate spends in the band ($\sim\tau_{TS}$), versus its electronic lifetime (τ_{EL}). Since τ_{TS} is effectively missing from M-LZ, the fact that M-LZ *qualitatively* matches our WP results in some limits (see eqs 11 and 18) is mainly fortuitous. In the M-LZ model we string probabilities of two-state transitions together that in reality are completely unconnected and which do not address energy spacing. Such an approach does capture some qualitative aspects of the irreversibility in the real SLI system because it incorporates a product of probabilities for large numbers of (independent classical) crossings that is analogous to that used, e.g., in constructing eq 11. But it obviously leaves out much of the fundamental physics, and LZ theory is therefore essentially incompatible with true SLI multistate models such as our WP models.

Implicit in our discussions above is that the LZ theory is very poorly equipped to address reduction. We saw in section 3 that the reduction κ depends on the electron impact time relative to the time the solvent brings the ET state into the band. One cannot enter any description of this complicated dynamics into the M-LZ model (recall the related difficulties of random trajectories through the band). Indeed, since M-LZ knows nothing of the DOS, the initial reduction state, an electron localized entirely within the semiconductor, is very problematic to represent within the M-LZ model. We have spoken above of M-LZ theory almost entirely in the context of oxidation because this is the only situation in which the initial state (all density localized in a discrete molecular state) can be adequately described.

There are many other effects that M-LZ cannot address. Back reactions/redistributions are improperly accounted for, as Appendix S.4 shows. Also the complex QI involved in multistate systems is completely unaddressed by M-LZ. Another effect peculiar to solid state systems is that they are capable of forming "surface molecules" which also can dramatically affect the charge transfer.[22,23,27,29,51] This surface molecule formation is highly dependent on the DOS of both the molecule and substrate, and thus LZ theory cannot account for any of these effects, which represent adsorption-mediated ET.

By this point it should be clear that the physics of the two-state LZ model, our M-LZ, and the higher level multistate models are in general very different. In a few rather contrived cases, such as some of those examined above (recall eq 20 is especially contrived), similar qualitative results sometimes emerge. However, given the vast differences in the underlying physics, we find in general that "agreement" is mainly fortuitous.

As we have discussed, the energy of the ET orbital is coupled to the conformational fluctuations of the solvent, and in turn the multipolar solvent responds to the changing charge distribution of the redox species. The latter is unaccounted for by our fixed nuclear trajectory in the 1D models. Within the TDAN model this can be accounted for by the boson term in eq 21 via the charge on the redox species (essentially $z - c_a^\dagger c_a$, where z is the ion charge when the orbital is unoccupied) and the linear coupling constant η_i (see eq 21). The coupling constant η_i is typically used in TDAN models to address coupling of a scattered atom or molecule to the solid's surface phonons. But η_i can also address the coupling of the redox species charge to the SLI polar solvent. Indeed, such boson terms are identical to some ET models,[47,52,53] as discussed in Appendix E. Tsukada's group has shown, using the TDAN Hamiltonian, eq 21, that the boson system can significantly affect the adiabaticity of the reaction[22,23,44,45] and cause deviations from the LZ P. This has been corroborated in a homogeneous ET application of the eq 21 Hamiltonian.[54] However this problem needs detailed investigation, especially the shortcomings of boson models, linear coupling constants, and terms linear in η_i, for addressing the coupling dynamics involved, and deficiencies in the TDAN description of the redox species' electronic structure and its electronic coupling to the solid and solvent. Examination of SLI ET nuclear/electronic coupling effects is a focus of our MO−MD[24,25] and our WPMD studies (see Appendix C).

VI. Conclusion

We believe our results show strong evidence that a two-state model cannot in general adequately address the many unique features of multistate systems such as the SLI. They suggest that the LZ outlook that dominates ET theory is of highly questionable utility for electrochemical systems. We believe they clearly show that the homogeneous κ cannot be applied in general to the SLI. Further, our discussions show that manifolds such as that in Figure 15 require careful scrutiny if physically meaningful conclusions are to be derived from them. In light of this it seems important to explore new avenues in theory building to model both real world SLI systems and new computer simulations. It appears our WPMD, as well as the TDAN model, should offer a rewarding approach. These models seem to us much better candidates for addressing and conceptualizing the multistate heterogeneous problem than traditional approaches. Traditional SLI ET theory does not contain a description of κ or address details of the SLI ET mechanism. We believe the WPMD model presented here offers a clear and detailed picture of the SLI ET mechanism, and that the 3D models are capable of addressing much of the SLI's rich dynamics. We have seen that the SLI κ can be calculated from our simulation methods, and we have elucidated its physics. Approximate analytical expressions for the SLI κ derived from our WP models will obviously (cf. eqs E.1-E.12) have a much more complicated form than those of LZ theory. We report such approximate expressions in another work (see eq 11 for the simplest example (oxidative) expression).[55]

As we have seen, our WPMD has direct analogies to TDAN models. However, the TDAN Hamiltonian is a simple model,

while WPMD is a true simulation method. Studies contrasting the two should be rewarding as many of their features are complementary, and we believe WPMD makes the physics of the SLI clearer than TDAN models.

There are a number of different quantum and semiclassical nonadiabatic MD simulation methods available to treat electronic transitions and the coupling between the nuclear and electronic system.[36,56−60] The semiclassical surface hopping trajectory (SHT) method[9,61−65] is currently one of the most popular. Tully originally formulated the SHT method for such a model Hamiltonian as in eq 21 (again, as for the TDAN model, for charge transfer associated with atoms/molecules scattered off UHV surfaces). The SHT simulation method is thus a natural choice to employ for SLI ET, and our WPMD method can be compared to it (especially regarding the various approximate means by which SHT addresses QI, see Appendix C).

We continue our comparison of traditional theory and the present one in another paper.[66] The process of reduction of SLI redox species, as shown in sections 3 and 4, consists of an incident beam of particles (electrons) being scattered into the SLI surface and near surface redox species. The natural language for this process is that of scattering theory, and it provides a means to analyze the rate process in terms of cross-sections. We address the second order SLI ET rate constants via cross-sections in the other paper.[66] In that paper we also look at the solvent dynamics effects on κ in greater detail, contrasting them with how such effects are addressed in homogeneous ET theory.

While our WPMD model clearly has advantages, a one-electron model has obvious shortcomings in the ultimate quest for a complete SLI model. ET is a dissociation event. Thus high level, many-electron correlation and exchange methods should be used for a complete description. One approach to such a goal are many-electron first principles MD simulations, such as those we are pursuing.[24,25] The challenge for the future lies in making high level SLI ET calculations computationally tractable, and also in developing conceptually helpful models for this complex system. It is our belief that the WPMD model takes steps toward meeting these two challenges.

Acknowledgment. This work was supported by the U.S. Department of Energy, Office of Basic Energy Sciences, Office of Energy Research, Division of Chemical Sciences.

Appendix

A. Further Examination of the LZ Model. As mentioned in the text, Landau and Zener assumed that the diabatic eigenstates ϵ_2 and ϵ_1 in eq 5 were a function of a single nuclear coordinate R and that this dependence was linear near the crossing region of the diabatic curves. By definition one has that

$$\mathrm{d}(\epsilon_2 - \epsilon_1)/\mathrm{d}t|_{\mathrm{Ro}} = (\mathrm{d}\epsilon_2/\mathrm{dR} - \mathrm{d}\epsilon_1/\mathrm{dR})\mathrm{d}R/\mathrm{d}t|_{\mathrm{Ro}} = (F_2 - F_1)v|_{\mathrm{Ro}} = \hbar\alpha \quad \text{(A.1)}$$

where $F_i = \mathrm{d}\epsilon_1/\mathrm{dR}$ are the forces at the intersection $\mathrm{R_o}$ of the diabatic curves, v is the nuclear velocity, and α is defined by eq 5 of the text. By using eq A.1 one can express γ in eq 7 as a function of F_i and v (instead of α as in eq 7)

$$\gamma = |V|^2/(\hbar|(\mathrm{d}(\epsilon_2 - \epsilon_1)/\mathrm{d}t|) = |V|^2/(\hbar^2\alpha) = |V|^2/(\hbar|(F_2 - F_1)|v) \quad \text{(A.2)}$$

The last equality of eq A.2 is often used in ET rate constant expressions in the fashion described next.

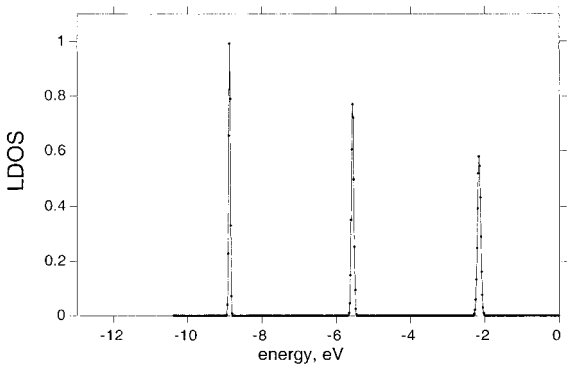

Figure 18. Figure 18. Local density of states on the redox species. Only $n = 6$, $n = 7$, $n = 8$ are shown for a value of V_o that placed the eigenvalues of these three states in the conduction band. The states are broadened energetically and shifted relative to their discrete values.

When eq A.2 is used in the ET context p can be calculated via eq 6 and eq A.2 since the forces arising from the curves and the appropriate nuclear velocity can be easily calculated from the simple quadratic model of ET theory.[4,11] One finds for the parameter γ, which fully specifies p (see eqs 6 and 7), that[12,35]

$$\gamma = [|V|^2\pi^{3/2}]/[(k_{\mathrm{B}}TE_{\mathrm{r}})^{1/2}\hbar\omega_{\mathrm{r}}] \quad \text{(A.3)}$$

where E_{r} is the reorganization energy.[4,11] A dependence of γ on E_{r} arises because the (free) energy curves F follow $\mathrm{F} = E_{\mathrm{r}}\mathrm{R}^2$, where R is the single reaction coordinate assumed in traditional ET models. R can be substituted for R in eqs A.1 and A.2.

The main assumptions of LZ theory are that[6−8] (1) the velocity v is constant in the region of R around point $\mathrm{R_o}$; (2) the diabatic states are linearly dependent on R and therefore also on t around $\mathrm{R_o}$ (so $\epsilon_2 - \epsilon_1 = \alpha t$); and (3) the electronic coupling matrix element $|V|$ is simply a constant (independent of t or R). The last two assumptions are consistent with the overall assumption that the transition occurs around a small region near the crossing point.

We have found that in SLI systems QI can significantly affect P. Our M-LZ model is not even qualitatively able to address these effects. This is to be compared with the two-state case where the LZ theory results roughly match higher level QI results, even though QI is unaccounted for in LZ theory.

B. Quasi-Stationary States, Gerischer Theory, Electronic Lifetimes. The density of states of the redox species is discrete if it is far from the surface, and we showed this DOS in Figure 2. But each of these discrete states acquires energy broadening when the redox species is sufficiently near the surface of the semiconductor because of coupling to the continuum of states in the semiconductor, in accord with well-known principles.[5] Let us place our five-atom molecule 3 Å from the center of the first semiconductor atom and set V_o such that the $n = 6$, $n = 7$, and $n = 8$ eigenvalues are in the conduction band. The resulting DOS of the redox species, i.e., its local DOS, is shown in Figure 18, and one sees each broadened (formerly discrete) state has an approximately Lorentzian shape (see Figure 18). The peaks of the Lorentzians also have their energy shifted relative to those of the isolated redox species, due to the coupling with the continuum.[20] The nearly perfect Lorentzian peaks in Figure 18 stem from the simple model we are presently discussing, and we have shown elsewhere that the broadening is complex for more realistic redox species.[24] The width of the Lorentzians in Figure 18 is directly related to the electronic lifetime of the various redox species states. That is, since there is energy broadening, the redox species states have a finite lifetime via

the energy−time uncertainty principle.[5,17,38,67] The electronic states of the redox species are now quasi-stationary states (they have finite lifetimes) versus the isolated redox species discrete eigenstates with infinite lifetimes.

This energy broadening Δ is itself energy dependent ($\Delta(\epsilon)$) and is directly related to the electronic coupling matrix element[24,25] and also to the discussion of lifetimes just given, as one can see by its formal definition[20]

$$\Delta(\epsilon) = \pi \sum_k |V_{ak}|^2 \delta(\epsilon - \epsilon_k) \quad \text{(B.1)}$$

The average electronic lifetime broadening of a state at an energy ϵ is approximately $\hbar/\Delta(\epsilon)$. We have discussed eq B.1 and SLI models for the energy dependence of $\Delta(\epsilon)$ elsewhere.[24,25] One sees from eq B.1 that this energy dependent broadening, $\Delta(\epsilon)$, is a projected density of states, i.e., the local density of states on the species next to the solid. One can thus express eq B.1 in terms of a DOS, and this is most easily done if an average coupling ($\langle |V_{ak}|^2 \rangle$) is assumed

$$\Delta(\epsilon) \approx \pi \langle |V_{ak}|^2 \rangle \sum_k \delta(\epsilon - \epsilon_k) = \pi \langle |V_{ak}|^2 \rangle \rho(\epsilon) \quad \text{(B.2)}$$

where $\rho(\epsilon)$ is generally modeled as a surface DOS.[20,21] The equations above have special relevance for TDAN models (see Appendix E).

Our ϵ_{RET} is not the same physical quantity as the energy levels of Gerischer's SLI ET theory, nor is our electronic broadening related to traditional theories' "solvent broadening".[16] Our ϵ_{RET} here simply denotes the energy at the peak of the Lorentzian associated with the redox species ET electron. There is no such electronic broadening in the Gerischer model; the electronic states are assumed to be discrete, i.e., the model for its "energy levels" is only applicable, at best, to redox species far separated from the electrode. The "broadening" of the "energy levels" in the Gerischer model is due to solvent fluctuations and has nothing to do with electronic broadening. This type of "solvent broadening" is also an inherent part of our model and simply stems from the Boltzmann activation energy term (cf. eq 9, and see refs 24 and 25).

C. WPMD Method. There are several modes in which we can run our WPMD simulation. The first and simplest regime propagates the nuclei using standard classical molecular dynamics (the pseudopotentials used are described in Appendix S.3 of the Supporting Information). When we identify a transition state (where the redox species eigenstate involved in the ET is in the band and the energy involved in ET is conserved) we save that configuration. Then the electron wave packet can be propagated in that fixed potential via the numerical method discussed in Appendix S.1. This is the equivalent of the frozen solvent regime in the 1D model. Actually, to bring energy conservation to within acceptable limits, the final MD TS solvent configuration is adjusted randomly using standard energy minimization techniques employing the time *independent* Schrödinger equation before wave packet propagation is performed.

We have various techniques to examine effects of solvent dynamics. In one dynamic solvent regime we simply allow the nuclear trajectory to be a fixed function of time (it is obtained from a fully classical MD simulation which ignores the changing charge distribution produced by the electronic dynamics). The nuclei are propagated in time steps of dt, and the electron is propagated for the same time via the Appendix S.1 method before the potential it sees is changed by a new nuclear configuration at the next time (t + dt). We have also experimented with propagating the nuclear trajectory for time dt, and the electron in time steps dt/N while interpolating the nuclear positions for the times spanning dt. All of these methods use the LZ assumption of a fixed classical trajectory. When electronic transitions are made in the simulation and energy is thus not conserved, the energy is redistributed to solvent modes by changing the solvent velocity at random. (The latter is the same as the most primitive of energy conservation techniques used in surface hopping trajectory methods.[9]) This technique can be used to see the degree to which LZ theory and related theories can describe systems which are idealized enough to render LZ an adequate description.

A final mode of our WPMD involves self-consistency between the nuclear and electron dynamics. As we mentioned in the text, self-consistent calculations for coupled quantum and classical systems are extremely computationally demanding. A number of techniques exist, with the surface hopping trajectory formalism being one of the most popular. When an avoided crossing is reached in these methods and a transition occurs across an energy gap, the interatomic forces are determined as a hybrid of the adiabatic forces for the lower and upper adiabatic surfaces. A variety of techniques are used to assign these forces and to redistribute "excess" energy to the solvent, with greater and lesser degrees of physical justification.[9] In our self-consistent mode we currently use Bohm trajectories with separation into "classical" and "quantum" forces and potentials.[68] However we only apply the method of Bohm to the nearest neighbor waters to the redox species. Any remaining excess energy is compensated for by changing the nuclear velocities of other bath water randomly. We are currently testing this method against surface hopping trajectory techniques and quantum results for simple systems. Results will be presented elsewhere. Numerous analogous hybrid simulations employing classical and quantum subsystems exist.[9,25,56−60] The ultimate check on such approximate simulations are full quantum mechanical simulations. That is partly why we have pursued fully quantum mechanical MO−MD and Car−Parrinello simulation methods.[24,25]

The pseudopotentials employed in our WPMD in this paper are discussed in the Supporting Information (Appendix S.3).

D. Multistate LZ Model (M-LZ). Let us first examine $\kappa =$ P for the normal ET regime in the multistate case. If we examine only one full crossing of the band of N states in Figures 15 and 16, one sees that the probability of forming products in any of the P_i wells starting from a given curve R_j is

$$P_1(R_j \Rightarrow P_i) \sim {p_o}^{(j-1)} \sum_{m=1}^{m=N} {p_o}^{m-1}(1 - p_o) = {p_o}^{j-1}(1 - p_M) \quad \text{(D.1)}$$

where we assume $p = p_M = {p_o}^N$. The ${p_o}^{(j-1)}$ term comes solely from lateral crossings and arises because every higher R_j curve in, e.g., Figure 16 has one more lateral crossing (along a "diabatic" pathway), of probability p_o for the path corresponding to each term in eq D.1. The probability of going, e.g, from R_1 to P_1 is $(1 - p_o)$; for R_1 to P_2 it is $p_o\,(1 - p_o)$ and so on, which forms the sum in eq D.1.

For two full crossings of the band the set of possible paths yields

$$P_2(R_j \Rightarrow P_i) \sim {p_o}^{j-1} \sum_{jo=1}^{jo=\infty} \sum_{m=1}^{m=N-1} {p_o}^N {p_o}^m (1 - p_o)^{(2(jo-1)+1)}$$

$$\approx {p_o}^{j-1} {p_o}^N p_o (1 - {p_o}^N) \approx {p_o}^{j-1} p_M (1 - p_M) \quad \text{(D.2)}$$

The p_o^N term in eq D.2 is the probability of ascent to the top. The path then descends with an adiabatic crossing of probability $1 - p_o$ followed by a "diabatic" crossing of probability p_o to the product curve P_N and so on, forming the sum. The term p_o^{j-1} appears in eq D.2 for the same reason as it appears in eq D.1. There can be any number of oscillatory crossings an odd number of times in the upper wells, hence the term $(1 - p^o)^{(2(jo-1)+1)}$ appears in eq D.2. These higher order oscillatory crossings do not contribute significantly to the sum except for small N, thus we truncate to only the jo=1 term to obtain the approximations shown in eq D.2. We use the fact that p_o is nearly 1 even for values of p_M close to zero for large N (because $p = p_M = p_o^N$) to obtain the last approximation of eq D.2. We consider back reactions in Appendix S.4. There are also other paths to products than those we have room to discuss, but none of these have very significant effects on P.

We have so far just described the probabilities for one and two full crossings of the band which give for the total P

$$P(R_j \Rightarrow P_i) = P_1 + P_2 \approx p_o^{j-1} p_M (1 - p_M) + p_o^{j-1}(1 - p_M) = p_o^{j-1}(1 - p_M^2) \quad \text{(D.3)}$$

If we have more than two full crossings of the band we find

$$P \approx p_o^{j-1}(1 - p_M N_F) \quad \text{(D.4)}$$

where N_F is the number of full crossings of the band and where we assume the same states are traversed in each of these full crossings, as we did above. Equation D.3 agrees with results in the solid-state literature;[43,45] however, the p_o^{j-1} factor does not appear because two crossing continuums are not considered in such literature.

To illustrate how eq D.4 is obtained let us assume $N_F = 4$, and disregard lateral crossings (only consider R_1). There are a large number of ways to perform four full crossings. We choose an expression which will lead to a pertinent path (one which does not end up in the initial reactant well at the end of a descent)

$$p_4 = p_o^N p_o^{N-1} p_o^{N-1} \sum_{j=1}^{j=N} p_o^2 p_o^{j-1}(1 - p_o) = p_M^3 - p_M^4 \quad \text{(D.5)}$$

(for $N_F = 4$) where p_4 stands for the probability of the four full crossings (we have omitted more than one oscillation in the upper wells). The path described by eq D.5 consists of a full ascent past P_1 to above P_N (along R_1), then a descent to the classical turning point above P_1, then "diabatic" ascent from this point to above P_N. Then, via the summation term over j, there are a series of descents to various product curves. Consideration of just four curves, for example, shows that the summation in eq D.5 can be envisioned as describing paths to curves P_3, P_2, P_1, P_4 for each term $j = 1$, $j = 2$, $j = 3$, $j = 4$ (respectively) in the sum in eq D.5 (the last path ($j = 4$) involves two recrossings). For any number of full crossings N_F it is easy to derive the analogous results to the last equality of eq D.5 and show that

$$P(R_1 \Rightarrow P_i) = p_1 + p_2 + p_3 + \ldots + p_{N_F} = \sum_{i=1}^{i=N_F} p_i = (1 - p_M) + (p_M - p_M^2) + (p_M^2 - p_M^3) + \ldots (p_M^{N_F - 1} - p_M^{N_F}) = 1 - p_M^{N_F} \quad \text{(D.6)}$$

Equation D.6 gives eq D.4 when lateral paths are considered.

To form the M-LZ equality shown in eq 20 a number of very restrictive approximations must hold. For example, the coupling, velocity, and forces must be the same at each intersection point. So that QI is not significant the coupling at all intersections must be small relative to the spacing between states. There must also be no time dependence involved for the coupling.

Many additional features of our M-LZ model are discussed in the Supporting Information section (appendix S.4). These include examination of the factor N_F, derivation of our equations for κ for the inverted ET region in the multistate case, and redistribution/back reaction paths in route to product wells.

E. TDAN Model. Let us first omit the boson term in eq 21, as in the text, and examine the remaining TDAN Hamiltonian. In the time dependent interaction representation one has[22,23,69]

$$i\hbar\partial/\partial t U(t, t_o) = V(t) U(t, t_o) \quad \text{(E.1)}$$

where V is (recall we are excluding the second line of eq 21)

$$V(t) = \exp[(i/\hbar)\int_t^{t_o} H_o(t)\, d\tau]\, V(t) \exp[-(i/\hbar)\int_t^{t_o} H_o(\tau')\, d\tau'] \quad \text{(E.2)}$$

$$H_o(t) = (\epsilon_{eff}(t)) c^\dagger_a c_a + \sum_k \epsilon_k c^\dagger_k c_k \quad \text{(E.3)}$$

$$V(t) = \sum_k (V_{ka}(t) c^\dagger_a c_k + V_{ak}(t) c^\dagger_k c_a) \quad \text{(E.4)}$$

The matrix elements of U (using the Hamiltonian of eq 21 minus the boson term) then satisfies the integro-differential equations shown next, which have been employed in numerous solid state works:[19,22,23,69]

$$\partial/\partial t\, U_{aa}(t, t_o) = -\int_{t_o}^{t} K(t, t')\, U_{aa}(t', t_o)\, dt' \quad \text{(E.5)}$$

$$\partial/\partial t\, U_{ak}(t, t_o) = -(i/\hbar) V'_{ak}(t) - \int_{t_o}^{t} K(t, t')\, U_{ak}(t', t_o)\, dt' \quad \text{(E.6)}$$

$$V'_{ak}(t) = V_{ak}(t) \exp[(i/\hbar)\int_{t_o}^{t} (\epsilon_{eff}(\tau) - \epsilon_k)\, d\tau] \quad \text{(E.7)}$$

$$K(t, t') = \hbar^{-2} \sum_k V_{ak}(t) V_{ka}(t') \exp[(i/\hbar)\int_{t_o}^{t} (\epsilon_{eff}(\tau) - \epsilon_k)\, d\tau] \quad \text{(E.8)}$$

The redox species orbital (adsorbate orbital in solid-state applications) occupation probability, i.e., expectation value, can thus be expressed as

$$n_{REDOX}(t) = \langle c_a^\dagger(t) c_a(t) \rangle = n_{REDOX}(t_o)|U_{aa}(t, t_o)|^2 + \sum_k n_k(t_o)|U_{ak}(t, t_o)|^2 \quad \text{(E.9)}$$

Now let us consider only conduction band ET and make some simplifying assumptions. First the time and k dependence of $V_{ka}(t)$ are assumed separable

$$V_{ka}(t) = u(t) V_{ka} \quad \text{(E.10)}$$

A central quantity which emerges from the TDAN and AN Hamiltonian is the energy broadening, $\Delta(\epsilon)$.[19,20] The physical meaning of this quantity and its defining equation (eq B.1) are given Appendix B. We have discussed eq B.1 and energy dependent SLI models for $\Delta(\epsilon)$ in detail.[24,25] But here for the TDAN model we assume the energy dependence of Δ is negligible so that we can approximate $\Delta(\epsilon)$ as the constant Δ_o.

We assume that the time dependence of Δ is described by the function u so that

$$\Delta(t) = \Delta_o u^2(t) \qquad \text{(E.11)}$$

The assumptions E.10 and E.11 have been used for many years in solid-state works.[70] Using eqs E.9−E.11 it can be shown that the occupation probability, $n_{\mathrm{REDOX}}(t)$, takes a form familiar from the solid-state literature[23,45]

$$n_{\mathrm{REDOX}}(t) = n_{\mathrm{REDOX}}(t_o) \exp(-2\int_{t_o}^{t} \Delta(t'')\, dt'') + (1/\pi\hbar) \int d\epsilon\, f(\epsilon, T) \times |\int_{t_o}^{t} (\Delta(t'))^{1/2} \exp[-i\epsilon t'/\hbar] \exp[(i/\hbar) \int_{t'}^{t} (i\epsilon_{\mathrm{eff}}(t'') + \Delta(t''))\, dt'']dt'|^2 \qquad \text{(E.12)}$$

where $f(\epsilon, T)$ is the Fermi−Dirac distribution function, t_o is the zero of time, and we assume that $\Delta(t)$ is given by eq E.11. Here, $n_{\mathrm{REDOX}}(t)$ has the same physical meaning as n_{REDOX} in the text.

If ϵ_{eff} and V_{ak} and V_{ka} have no time dependence and $n_{\mathrm{REDOX}}(t = 0) = 1$ and $n_k(t = 0) = 0$, then it is easy to show from eqs E.12 or E.9 and B.1 that we have the simple oxidative exponential decay of the redox species state into the continuum of semiconductor states discussed in the text

$$n_{\mathrm{REDOX}}(t) = n_{\mathrm{REDOX}}(t_o) \exp(-\Delta_o t/\hbar) \qquad \text{(E.13)}$$

However, in general, $n_{\mathrm{REDOX}}(t)$ can have very complicated time dependence even if $\epsilon_{\mathrm{eff}}(t)$ and $\Delta(t)$ have simple time dependence.[19,22,23] Equation E.12 gives the LZ result for two state models in regimes in which the LZ assumptions hold when equations such as eq 10 are used for $\epsilon_{\mathrm{eff}}(t)$.[45] We find it gives results for the multistate $P = \kappa$ that agree roughly with our 1D model of the text. The TDAN model is a lower level model than our WPMD (see text, section 6). P is simply $n_{\mathrm{REDOX}}(t\rightarrow\infty)$ of eq E.12, where this long time limit has the same meaning as in section 2, and multiple crossings can be involved.

The boson term in eq 21 has close connections to those used in homogeneous models for ET. This boson term is analogous to spin-Boson Hamiltonian ET models.[52,71] These models too involve a linear coupling of the redox species to a solvent bath, and the solvent is also, of course, represented by a collection of harmonic oscillators. Tsukada's group has presented solutions for the TDAN model with the boson term.[22,23,44] Previous solid−liquid ET studies (e.g., refs 13 and 47) have used the time independent version of eq 21 in a time independent Schrödinger equation, and the implications of the TDAN studies for the ET κ have not been reported in these. The main implication is that significant differences arise with respect to the LZ P, even for two-state systems.[22,23,44]

References and Notes

(1) Meier, A.; Selmarten, D.; Siemoneit, K.; Smith, B. B.; Nozik, A. J. *J. Phys. Chem. B* **1999**, *103*, 2122.

(2) Miller, R. J. D.; McLendon, G. L.; Nozik, A. J.; Schmickler, W.; Willig, F. *Surface Electron Transfer Processes*; VCH Publishers: New York, 1995.

(3) Cohen, M. L.; Chelikowsky, J. R. *Electronic Structure and Optical Porperties of Semiconductors*; Springer-Verlag: New York, 1988; Vol. 75.

(4) Marcus, R. A. *J. Chem. Phys.* **1964**, *15*, p 155.

(5) Cohen-Tannoudji, C.; Diu, B.; Laloe, F. *Quantum Mechanics*; John Wiley and Sons: Paris, 1977.

(6) Zener, C. *Proc. R. Soc. London* **1932**, *A137*, 696.

(7) Landau, L. D. *Physik. Zeitschr. Sowjetunion* **1932**, *2*, 46.

(8) Baede, A. P. M. *Adv. Chem. Phys.* **1975**, *30*, 463.

(9) Coker, D. F. *Computer Simulation Methods for Nonadiabatic Dynamics in Condensed Systems*; Allen, M. P., Tildesley, D. J., Eds.; Kluwer: Dordrecht, 1993; p 315.

(10) Stueckelberg *Helv. Phys. Acta* **1932**, *5*, 370.

(11) Marcus, R. A. *J. Chem. Phys.* **1965**, 679.

(12) Newton, M. D. *Chem. Rev.* **1991**, *91*, 767.

(13) Smith, B. B.; Hynes, J. T. *J. Chem. Phys.* **1993**, *99*, 6517.

(14) Newton, M. D.; Sutin, N. *Annu. Rev. Phys. Chem.* **1984**, *35*, 437.

(15) Obviously, we have been discussing expressions for the local rate constant for ET between the semiconductor and the redox species (see eq 10). This k has units of s^{-1} and is thus a first order rate constant. In the semiconductor−liquid case the full rate constant is generally assumed second order, being assumed dependent on the concentration of redox molecules and electrons/holes. We discuss this second order rate constant in detail elsewhere in the context of the scattering language that arises naturally from our WPMD model.[66] We have discussed this second order rate constant from other perspectives elsewhere.[24,25]

(16) Morrison, S. R. *Electrochemistry of Semiconductors and Oxidized Metal Electrodes*; Plenum Press: New York, 1980.

(17) Schiff, L. I. *Quantum Mechanics*; 3rd ed.; McGraw-Hill: New York, 1968.

(18) Bohm, D. *Quantum Theory*; Dover: New York, 1951.

(19) Brako, R.; Newns, D. M. *Surf. Sci.* **1981**, *108*, 253.

(20) Muscat, J. P.; Newns, D. M. *Prog. Surf. Sci.* **1978**, *9*, 1.

(21) Newns, D. M. *Phys. Rev.* **1969**, *178*, 1123.

(22) Tsukada, M.; Shima, N.; Tsuneyuki, S. *Prog. Surf. Sci.* **1987**, *26*, 47.

(23) Tsukada, M. *Theory of Dynamic Processes of Surfaces*; Tamaru, K., Ed.; Plenum Press: New York, 1993; p 29.

(24) Smith, B. B.; Nozik, A. J. *Chem. Phys.* **1996**, *205*, 47.

(25) Smith, B. B.; Nozik, A. J. *J. Phys. Chem. B* **1997**, *101*, 2459.

(26) Herman, M. F. *J. Chem. Phys.* **1985**, *82*, 3666.

(27) Zangwill, A. *Physics at Surfaces*; Cambridge University Press: New York, 1989.

(28) Sze, S. M. *Physics of Semiconductor Devices*; John Wiley and Sons: New York, 1981.

(29) Davidson, S. G.; Levine, J. D. *Solid State Phys.* **1970**, *25*, 1.

(30) Smith, B. B.; Nozik, A. J. **1999**, to be submitted to *J. Chem. Phys.*

(31) Curtiss, L. A.; Halley, J. W.; Hautman, J.; Nagy, Z.; Rhee, Y.-J.; Yonco, R. M. *J. Electrochem. Soc.* **1991**, *138*, 2032.

(32) Kuharski, R.; Bader, J.; Chandler, D.; Sprik, M.; Klein, M.; Impey, R. *J. Chem. Phys.* **1988**, *89*, 3248.

(33) Hautman, J.; Halley, J. W.; Rhee, Y.-J. *J. Chem. Phys.* **1989**, *91*, 467.

(34) Elliott, S. R. *Physics of Amorphous Materials*; Longman: London, 1984.

(35) Kuznetsov, A. M.; Ulstrup, J.; Vorotyntsev, M. A. *Solvent Effects in Charge Transfer Processes*; al., R. R. D. e., Ed.; Elsevier: Amsterdam, New York, 1985; Vol. C, p 163.

(36) Wolynes, P. G. *J. Chem. Phys.* **1987**, *87*, 6559.

(37) Sebastian, K. L. *J. Chem. Phys.* **1989**, *90*, 5056.

(38) Taylor, J. R. *Scattering Theory: The Quantum Theory of Nonrelativistic Collisions*; Robert E. Krieger Pub. Co., Inc.: Malabar, Florida, 1987.

(39) Ricca, F. *Adsorption−desorption phenomena*; Academic Press: New York, 1972.

(40) Ferry, D. *Quantum Transport in Semiconductors;* Wiley: New York, 1992.

(41) Economou, E. N. *Green's Functions in Quantum Physics*; Springer-Verlag: Berlin, 1983.

(42) Desjonqueres, M. C.; Spanjaard, D. *Concepts in Surface Physics*; Springer-Verlag: Heidelberg, 1993.

(43) Demkov, Y. N.; Osherov, V. I. *Soviet Phys. − JETP* **1968**, *29*, 916.

(44) Tsukada, M. *J. Phys. Soc. Jpn.* **1982**, *51*, 2927.

(45) Tsuneyuki, S.; Shima, N.; Tsukada, M. *Surf. Sci.* **1987**, *186*, 26.

(46) Boroda, Y. G.; Voth, G. A. *J. Chem. Phys.* **1996**, *104*, 6168.

(47) Schmickler, W. *J. Electroanal. Chem.* **1986**, *204*, 31.

(48) Smith, B. B.; Koval, C. A. *J. Electroanal. Chem.* **1990**, *277*, 43.

(49) Smith, B. B.; Staib, A.; Hynes, J. T. *Chem. Phys.* **1993**, *176*, 521.

(50) Zichi, D. A.; Ciccotti, G.; Hynes, J. T.; Ferrario, M. *J. Phys. Chem.* **1989**, *93*, 6261.

(51) Davidson, S. G.; Huang, Y. S. *Solid State Commun.* **1974**, *15*, 863.

(52) Garg, A.; Onuchic, J. N.; Ambegaokar, V. *J. Chem. Phys.* **1985**, *83*, 4491.

(53) Chandler, D. *J. Stat. Phys.* **1986**, *42*, 49.

(54) Zhen, Y. *Mod. Phys. Lett.* **1988**, *2*, 743.

(55) Smith, B. B.; Nozik, A. J. *in preparation.*

(56) Baer, M. The Theory of Electronic Nonadiabatic Transitions in Chemical Reactions. In *Theory of Chemical Reaction Dynamics*; Baer, M., Ed.; CRC: Boca Raton, 1985; Vol. II, p 219.

(57) Pechukas, P. *Phys. Rev.* **1969**, *181*, 174.

(58) Nakamura, H. *J. Chem. Phys.* **1987**, *87*, 4031.

(59) Dehareng, D. *Chem. Phys.* **1986**, *110*, 375.

(60) Sawada, S.; Metiu, H. *J. Chem. Phys.* **1986**, *84*, 227.

(61) Blais, N. C.; Truhlar, D. G.; Mead, C. A. *J. Chem. Phys.* **1988**, *89*, 6204.

(62) Herman, M. F.; Kluk, E. *Chem. Phys.* **1984**, *91*, 27.

(63) Miller, W. H. *Adv. Chem. Phys.* **1974**, *25*, 69.

(64) Tully, J. C. Nonadiabatic Processes in Molecular Collisions. In *Dynamics of Molecular Collisions*; Miller, W. H., Ed.; Plenum: New York, 1976; p 217.

(65) Tully, J. C.; Preston, R. K. *J. Chem. Phys.* **1971**, *55*, 562.

(66) Smith, B. B.; Nozik, A. J. *J. Phys. Chem. B* **1999**.

(67) Landau, L. D.; Lifshitz, E. M. *Quantum Mechanics*; Pergamon Press: New York, 1977.

(68) Holland, P. R. *The Quantum Theory of Motion*; Cambridge University Press: New York, 1993.

(69) Zheng, X. M.; Smith, P. V. *Surf. Sci.* **1992**, *279*, 127.

(70) Bloss, W.; Hone, D. *Surf. Sci.* **1978**, *72*, 277.

(71) Bader, J. S.; Kuharski, R. A.; Chandler, D. *J. Chem. Phys.* **1990**, *93*, 230.